Identification of V. parvula and S. gordonii adhesins mediating co-aggregation and its impact on physiology and mixed biofilm structure

Louis Dorison, Nathalie Béchon, Camille Martin-Gallausiaux, Susan Chamorro-Rodriguez, Yakov Vitrenko, Rania Ouazahrou, Romain Villa, Julien Deschamps, Romain Briandet, Simonetta Gribaldo, et al.

To cite this version:

Louis Dorison, Nathalie Béchon, Camille Martin-Gallausiaux, Susan Chamorro-Rodriguez, Yakov Vitrenko, et al.. Identification of V. parvula and S. gordonii adhesins mediating co-aggregation and its impact on physiology and mixed biofilm structure. 2024. hal-04659886

HAL Id: hal-04659886
https://hal.inrae.fr/hal-04659886v1

Preprint submitted on 23 Jul 2024

HAL is a multi-disciplinary open access archive for the deposit and dissemination of scientific research documents, whether they are published or not. The documents may come from teaching and research institutions in France or abroad, or from public or private research centers.

L'archive ouverte pluridisciplinaire **HAL**, est destinée au dépôt et à la diffusion de documents scientifiques de niveau recherche, publiés ou non, émanant des établissements d'enseignement et de recherche français ou étrangers, des laboratoires publics ou privés.

Distributed under a Creative Commons Attribution - NonCommercial - NoDerivatives 4.0 International License

bioRxiv preprint doi: https://doi.org/10.1101/2024.07.16.603716; this version posted July 16, 2024. The copyright holder for this preprint (which was not certified by peer review) is the author/funder, who has granted bioRxiv a license to display the preprint in perpetuity. It is made available under aCC-BY-NC-ND 4.0 International license.

1 # Identification of *V. parvula* and *S. gordonii* adhesins mediating co-
2 aggregation and its impact on physiology and mixed biofilm
3 structure.
4
5 Louis Dorison[1], Nathalie Béchon[1, 3], Camille Martin-Gallausiaux[2], Susan Chamorro-
6 Rodriguez[1], Yakov Vitrenko[4], Rania Ouazahrou[4], Romain Villa[2], Julien Deschamps[5],
7 Romain Briandet[5], Simonetta Gribaldo[2], Jean-Marc Ghigo[1], and Christophe Beloin*[1]
8
9 [1] Institut Pasteur, Université Paris Cité, Genetics of Biofilms Laboratory, CNRS
10 UMR6047, 75015 Paris, France
11 [2] Institut Pasteur, Université Paris Cité, Evolutionary Biology of the Microbial Cell La-
12 boratory, CNRS UMR6047, 75015 Paris, France.
13 [3] Present address: Department of Molecular Genetics, Weizmann Institute of Science,
14 Rehovot 7610001, Israel
15 [4] Institut Pasteur, Université Paris Cité, C2RT, Biomics Technology Plateform, 75015,
16 Paris, France
17 [5] Université Paris-Saclay, Institut national de recherche pour l'agriculture, l'alimenta-
18 tion et l'environnement (INRAE), AgroParisTech, Micalis Institute, Jouy-en-Josas
19 78350, France
20
21
22 ***Corresponding authors:**
23 christophe.beloin@pasteur.fr (ORCID: 0000-0002-0344-3443)
24
25 **Keywords:** Veillonella, Streptococcus, adhesin, dental plaque, trimeric autotrans-
26 porter, aggregation, coaggregation.
27
28
29
30
31
32
33
34
35
36
37
38
39
40
41
42
43
44
45
46
47
48
49

bioRxiv preprint doi: https://doi.org/10.1101/2024.07.16.603716; this version posted July 16, 2024. The copyright holder for this preprint (which was not certified by peer review) is the author/funder, who has granted bioRxiv a license to display the preprint in perpetuity. It is made available under aCC-BY-NC-ND 4.0 International license.

ABSTRACT

The dental plaque is a polymicrobial community where biofilm formation and co-aggregation, the ability to bind to other bacteria, play a major role in the construction of an organized consortium. One of its prominent members is the anaerobic diderm *Veillonella parvula,* considered as a bridging species, which growth depends on lactate produced by oral *Streptococci*. Understanding how *V. parvula* co-aggregates and the impact of aggregation has long been hampered due to the lack of appropriate genetic tools. Here we studied co-aggregation of the naturally competent strain *V. parvula* SKV38 with various oral bacteria and its effect on cell physiology. We show that *V. parvula* requires different trimeric autotransporters of the type V secretion system to adhere to oral *Streptococci* and *Actinomyces*. In addition, we describe a novel adhesin of *Streptococcus gordonii,* VisA (SGO_2004), as the protein responsible for co-aggregation with *V. parvula*. Finally, we show that co-aggregation does not impact cell-cell communication, which is mainly driven by environmental sensing, but plays an important role in the architecture and species distribution within the biofilm.

bioRxiv preprint doi: https://doi.org/10.1101/2024.07.16.603716; this version posted July 16, 2024. The copyright holder for this preprint (which was not certified by peer review) is the author/funder, who has granted bioRxiv a license to display the preprint in perpetuity. It is made available under aCC-BY-NC-ND 4.0 International license.

92 **INTRODUCTION**

93

94 Bacterial attachment to other bacteria is a key step in the formation of bacterial
95 biofilm. This adhesion is termed auto-aggregation when the adhesion occurs with a
96 genetically identical bacteria and co-aggregation when different species or strains are
97 involved. While auto-aggregation is known to enhance stress resistance, antibiotic tol-
98 erance, and virulence, the specific role of co-aggregation remains largely understud-
99 ied[1], except in the contexts of the dental plaque and certain aquatic environments[2–4].
100 The dental plaque is an important polymicrobial biofilm whose perturbation can
101 lead to the development of caries and periodontitis[5,6]. The formation of the dental
102 plaque is a stepwise process which begins with the adhesion to the teeth surface of
103 early colonizers comprised of oral streptococci, including *Streptococcus gordonii, S.*
104 *oralis* and *S. mitis* and *Actinomyces spp.*. Then, bridging species such as *Veillonella*
105 and *Fusobacterium* co-aggregate with the early colonizers forming an adhesion sub-
106 strate for late biofilm commensal colonizers but also the opportunistic pathogens *Por-*
107 *phyromonas gingivalis*, *Treponema denticola* and *Tannerella forsythia*[2]. Co-aggrega-
108 tion is mostly driven by adhesins [7–12], few of which have been identified, including *P.*
109 *gingivalis* major and minor fimbriae[13,14], which interacts with *S. gordonii* SspB adhesin
110 and GADPH, and the *F. nucleatum* autotransporters RadD and Fap2 [9,11,15]. However,
111 most of the molecular actors of oral biofilm co-aggregation mechanisms are currently
112 unknown.
113 *Veillonella* are strict anaerobic diderm firmicutes and seven *Veillonella* species
114 can be found in the dental plaque[16] where they rely on lactate produced by oral strep-
115 tococci as a carbon source[17]. Oral *Veillonella* species possess extensive aggregative
116 properties contributing to their colonization of the oral environment [7] in which the phys-
117 ical proximity resulting from aggregation with their different partners likely facilitates
118 their metabolic integration in the oral biofilm. For instance, *V. parvula* (previously *V.*
119 *atypica*) strain PK1910 induces the expression of the *S. gordonii* amylase *amyB* in a
120 distance-dependent manner, possibly to increase lactic acid production[18,19]. *V. atypica*
121 was also shown to produce a catalase protecting *F. nucleatum* from reactive oxygen
122 species produced by *S. gordonii*[20].
123 While *Veillonella* adhesive properties have been first characterized more than
124 30 years ago [21,22], the underlying molecular actors of co-aggregation and its

bioRxiv preprint doi: https://doi.org/10.1101/2024.07.16.603716; this version posted July 16, 2024. The copyright holder for this preprint (which was not certified by peer review) is the author/funder, who has granted bioRxiv a license to display the preprint in perpetuity. It is made available under aCC-BY-NC-ND 4.0 International license.

125 physiological consequences remained elusive until recently. Indeed, it was recently
126 shown that *V. atypica* OK5 possesses eight trimeric autotransporter adhesins (TAA)
127 belonging to the type Vc secretion system family. One of them, Hag1, mediates adhe-
128 sion to oral bacteria and buccal cells[23]. On the other side, several oral *Veillonella* spe-
129 cies, including *V. atypica* OK5, co-aggregate with *S. gordonii* Hsa adhesin[24]. However,
130 a more extensive mechanistic characterization of the *Veillonella* adhesin repertoire
131 was hampered due to the lack of genetic tools described for this genus. *V. parvula*
132 strain SKV38 is a recently described naturally competent isolate that is readily genet-
133 ically engineered[25]. We have recently shown that it possesses nine TAAs, named VtaA
134 to -I, and 3 classical monomeric autotransporters, named VmaA to -C. Both VtaA and
135 a gene cluster coding for 8 TAA adhesins were shown to be important for surface ad-
136 hesion and biofilm formation[25].

137 Here, we investigated the capacity of *V. parvula* SKV38 to co-aggregate with
138 common oral bacteria and studied the physiological impact of this co-aggregation. We
139 found that, in addition to mediating auto-aggregation, VtaA is also involved in co-ag-
140 gregation with *S. oralis* while two other adhesins encoded in an adhesin cluster, VtaE
141 and VtaD, are involved in co-aggregation with *S. gordonii* and *Actinomyces oris*. We
142 also identified a novel adhesin of *S. gordonii*, VisA (SGO_2004), as the possible inter-
143 acting partner of *V. parvula* VtaE/VtaD. Analysis of the transcriptomic profiles of both
144 bacteria in coculture with or without aggregation suggested a very limited impact of
145 aggregation on gene expression. Furthermore, we showed that absence of co-aggre-
146 gation results in spatial segregation of the two species biofilms, suggesting that co-
147 aggregation would be necessary to generate the architecture of a healthy dental
148 plaque biofilm. In conclusion, this study contributes to provide a better mechanistic
149 understanding of co-aggregation between oral bacteria, one of the key organization
150 principles driving dental plaque formation.

151
152
153
154
155
156
157
158
159
160

bioRxiv preprint doi: https://doi.org/10.1101/2024.07.16.603716; this version posted July 16, 2024. The copyright holder for this preprint (which was not certified by peer review) is the author/funder, who has granted bioRxiv a license to display the preprint in perpetuity. It is made available under aCC-BY-NC-ND 4.0 International license.

161 # RESULTS

162

163 ***V. parvula* uses specific adhesins to interact with *S. oralis*, *S. gordonii* and *A.*
164 *oris*.**

165 In order to identify potential ligands of *V. parvula* SKV38 adhesins, we used our
166 model *V. parvula* SKV38 strain to perform co-aggregation assays with different
167 bacterial members of the dental plaque. *V. parvula* SKV38 co-aggregated with several
168 *Streptococcus gordonii* strains, *Streptococcus oralis* ATCC10557 and *Actinomyces*
169 *oris* CIP102340. It did not, however, co-aggregate with *Streptococcus mitis* CIP
170 104996, *Streptococcus parasanguinis* CIP104372T, *Fusobacterium nucleatum* ATCC
171 25586 and *Streptococcus mutans* NG8, UA159, CBSm8 and CBSm38 and only very
172 weakly with *S. mutans* UA140 (Figure 1A, Figure S1). We decided to further investigate
173 the determinant of co-aggregation between *V. parvula* SKV38 and *S. oralis* ATCC
174 10557*, S. gordonii DL1* and *A. oris* CIP102340. To identify which of the 12 *V. parvula*
175 adhesins were involved in the co-aggregation with these different partners, we used
176 previously constructed single deletion mutants of each of these adhesins[25] and
177 performed co-aggregation assays by mixing independent cultures of each of the three
178 tested oral bacterial strain and the 12 *V. parvula* adhesin mutants in aggregation buffer.
179 Deletion of *V. parvula* trimeric autotransporter VtaA abolished co-aggregation with *S.*
180 *oralis,* while deletion of the trimeric autotransporter VtaE abolished co-aggregation with
181 *S. gordonii* and strongly reduced co-aggregation with *A. oris* (Figure 1B-E and S2). A
182 double mutant lacking both VtaA and VtaE showed reduced co-aggregation with *A.*
183 *oris* compared to a *ΔvtaE* single mutant, suggesting that VtaA is a secondary adhesin
184 involved in the co-aggregation with *A. oris* (Figure 1G). Microscopy observation of *V.*
185 *parvula* incubated with *S. oralis, S. gordonii* and *A. oris* confirmed the observed co-
186 aggregation phenotypes (Figure S2). Moreover, use of P_{Tet}-*vtaA* or P_{Tet}-*vtaE*
187 constructs, in which the chromosomal *vtaA* and *vtaE* genes are placed under the
188 control of an aTc inducible promoter, allowed us to recapitulate the aggregative
189 phenotype in an aTc-dependent manner (Figure 1C-E). Both the P_{Tet}-*vtaA* and the P_{Tet}-
190 *vtaE* strains partially co-aggregated with *S. oralis* and *A. oris*, even in absence of aTc,
191 suggesting a leakage of the used P_{Tet} promoter. While deletion of *vtaE* completely
192 abolished co-aggregation with *S. gordonii* when mixed after independent growth, it only
193 partially abrogated co-aggregation with *S. gordonii* when cocultured overnight (Figure

bioRxiv preprint doi: https://doi.org/10.1101/2024.07.16.603716; this version posted July 16, 2024. The copyright holder for this preprint (which was not certified by peer review) is the author/funder, who has granted bioRxiv a license to display the preprint in perpetuity. It is made available under aCC-BY-NC-ND 4.0 International license.

194 1F), suggesting that another *V. parvula* adhesin could contribute to co-aggregation.
195 Consistently, we identified VtaD as being this secondary adhesin, since any residual
196 co-aggregation between *S. gordonii* and *V. parvula* disappeared in the Δ*vtaCDEF* and
197 Δ*vtaDE* mutants (Figure 1F). *vtaD* is the gene located immediately upstream of *vtaE*
198 and VtaD has a high similarity to VtaE (81%), which may explain why both
199 corresponding proteins possess similar binding activities. However, *vtaD* encodes a
200 shorter adhesin than VtaE (2071 residues opposed to 3141 residues), mostly lacking
201 part of the repetitive sequences found in *vtaE* stalk (Figure S3 and S4). Interestingly,
202 deletions of *vtaC* or *vtaF* in the Δ*vtaE* background increased the aggregative
203 phenotype of *V. parvula* with *S. gordonii* (Figure 1F) suggesting that these other
204 adhesins may interfere with the VtaD-dependent co-aggregation process.
205

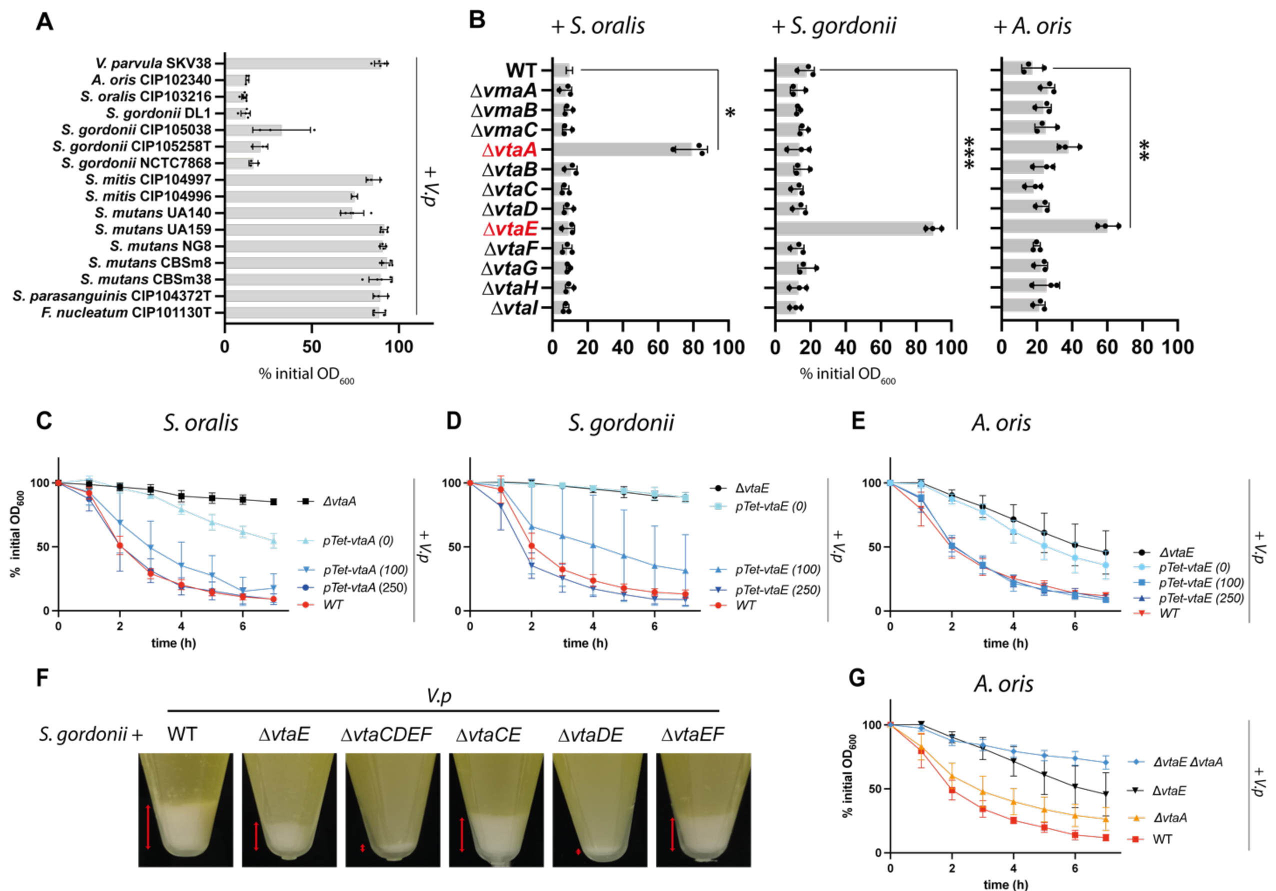

206

207 **Figure 1: VtaA and VtaE are the adhesins responsible for co-aggregation with**
208 ***S. oralis, S. gordonii and A. oris.***
209 (A) Co-aggregation of independent cultures of both *V. parvula* SKV38 and various members of the dental
210 plaque after 7h, as measured by the % of decrease of optical density between 0 and 7h. SD and single
211 points for 3-5 replicates are shown. See Figure S1 for auto-aggregation of each strain. (B) Aggregation
212 of *V. parvula* SKV38 WT and each single autotransporter mutant with *S. oralis ATCC 10557, S. gordonii*

bioRxiv preprint doi: https://doi.org/10.1101/2024.07.16.603716; this version posted July 16, 2024. The copyright holder for this preprint (which was not certified by peer review) is the author/funder, who has granted bioRxiv a license to display the preprint in perpetuity. It is made available under aCC-BY-NC-ND 4.0 International license.

DL1 and *A. oris* CIP102340 after 7h. SD and single points for 3 replicates are shown. The indicated p-values were calculated by comparing all conditions to the partner + *Vp* WT using a Brown-Forsythe and Welch ANOVA followed by Dunnett correction. (C-E and G) Co-aggregation curves of *V. parvula* WT, Δ*vtaA*, Δ*vtaE*, Δ*vtaE*Δ*vtaA* and P_{Tet} -*vtaE* or P_{Tet} -*vtaA* with 0, 100 or 250 ng/ µl of aTc. Curves represent the mean and SD of 6-17 replicates. (F) Representative pictures of co-aggregates after coculture between *S. gordonii* WT and *V. parvula* WT and different adhesin mutants; red arrow bars indicate the relative size of the aggregated fraction.

The Hag1 trimeric autotransporter has been shown to be involved in the adhesion of *V. atypica* OK5 to human oral epithelial cells[23]. Interestingly, the genes encoding VtaA and Hag1 are located at the same locus on the genome of *V. parvula* SKV38 and *V. atypica* OK5, respectively, with the difference that Hag1 is preceded by another trimeric adhesin. Comparison of this locus among different *Veillonella* revealed that this locus always contains adhesins, although the number of adhesin and their identity differs between strains, even within the same species (Figure S5). This feature is reminiscent of *V. parvula* SKV38[25] cluster of adhesin that is also present in a locus that consistently hosts diverse adhesins across *Veillonella* species.

Apart from its importance in the dental plaque, *V. parvula* is also present throughout the gastrointestinal tract. We wondered whether some of its adhesins are involved in adhesion to oral or intestinal cells, rather than other bacteria. In contrast to the known strong interaction between *V. atypica* and host cells[23], we observed only a moderate adhesion of *V. parvula* SKV38 to TR146 oral and Caco-2 intestinal epithelial cells using microscopy (Figure S6 A-C). We then tested whether the major adhesins of *V. parvula* were involved in this interaction using a Δ*vtaCDEF*Δ*vtaA* mutant.. Deletion of the large adhesin group did not reduce adhesion to either cell type. Finally, we examined whether the other adhesins of *V. parvula* SKV38 could impact Caco-2 cell adhesion, and showed that there were no significant differences in adhesion (Figure S6D).

Identification of VisA (*SGO_2004*), a new *S. gordonii* adhesin mediating co-aggregation with *V. parvula*.

To further characterize the molecular actors of co-aggregation, we focused on the pair *V. parvula / S. gordonii* and took advantage of a recently published collection

bioRxiv preprint doi: https://doi.org/10.1101/2024.07.16.603716; this version posted July 16, 2024. The copyright holder for this preprint (which was not certified by peer review) is the author/funder, who has granted bioRxiv a license to display the preprint in perpetuity. It is made available under aCC-BY-NC-ND 4.0 International license.

250 of 27 *S. gordonii* DL1 surface proteins deletion mutants[26], corresponding to all 26
251 LPXTG cell wall anchor domain-containing proteins plus two mutants of the Amylase-
252 binding protein A (AbpA) and B (AbpB). We first investigated co-aggregation between
253 wild-type *V. parvula* and all *S. gordonii* mutants and we identified two mutants, Δ*padA*
254 (*SGO_2005*) and Δ*SGO_2004*, presenting either a reduced (Δ*padA*) or total loss of co-
255 aggregation (Δ*SGO_2004*) with *V. parvula* (Figure 2A-B).

256 *padA* and *SGO_2004* are part of an operon (Figure 2D) and the observed loss
257 of aggregation in the Δ*padA* mutant could be due to a polar effect on the downstream
258 *SGO_2004* gene[27]. To test for this hypothesis, we inserted a P_{Tet} inducible promoter
259 with the pVeg RBS [28] upstream of *SGO_2004,* while retaining or deleting the *padA*
260 gene. In both cases, co-aggregation was fully recovered in presence of aTc (Figure
261 2C), demonstrating that SGO_2004 alone is the protein responsible for *S. gordonii* co-
262 aggregation with *V. parvula*. *SGO_2004* is a gene of previously unknown function cod-
263 ing for an 807 amino acid protein composed of a flexible chain of disordered/poorly
264 predicted 3 short alpha helixes, 7 G5-domains and an LPXTG domain (Figure 2D-E).
265 Homologues of this protein are found in other, sometime distant, Streptococci, next to
266 a *padA* homologue (Figure S7). Considering its newly identified role, we renamed this
267 new aggregation-mediating adhesin VisA, for **V**eillonella **I**nteracting **S**treptococcal
268 protein A.
269

270 ## *S. gordonii* VisA directly interacts with *V. parvula* VtaE and VtaD
271

272 To determine whether co-aggregation mediated by *V. parvula* VtaE and VtaD and
273 *S. gordonii* VisA resulted from direct or indirect interactions, we purified the VisA region
274 containing its 7 G5 domains (residues 138-698 with a C-terminal His-tag, see Figure
275 2D) in *E. coli* and used the purified protein to assess potential direct interactions with
276 *V. parvula*. When used at a concentration above 1µg/mL, $VisA_{G5}$ was sufficient to
277 induce aggregation of *V. parvula* on its own (Figure 3A). Confirming our previous
278 observations, a Δ*vtaE* mutant retained a partial aggregation phenotype, while a Δ*vtaD-*
279 *vtaE* mutant did not, and Δ*vtaE*Δ*vtaC* and Δ*vtaE*Δ*vtaF* mutants displayed an
280 intermediate phenotype (Figure 3B). Moreover, immunofluorescence using an anti-His
281 antibody detecting $VisA_{G5}$ incubated with *V. parvula* WT, Δ*vtaE* or Δ*vtaD-vtaE* showed
282 that while $VisA_{G5}$ could be detected at the surface of *V. parvula* WT (Figure 3C) or

bioRxiv preprint doi: https://doi.org/10.1101/2024.07.16.603716; this version posted July 16, 2024. The copyright holder for this preprint (which was not certified by peer review) is the author/funder, who has granted bioRxiv a license to display the preprint in perpetuity. It is made available under aCC-BY-NC-ND 4.0 International license.

283 ΔvtaE (Figure 3D), no signal could be seen for the ΔvtaD-vtaE mutant (Figure 3E).
284 Altogether, these results suggested that VisA binds to *V. parvula* surface via a direct
285 interaction with VtaE or VtaD.
286

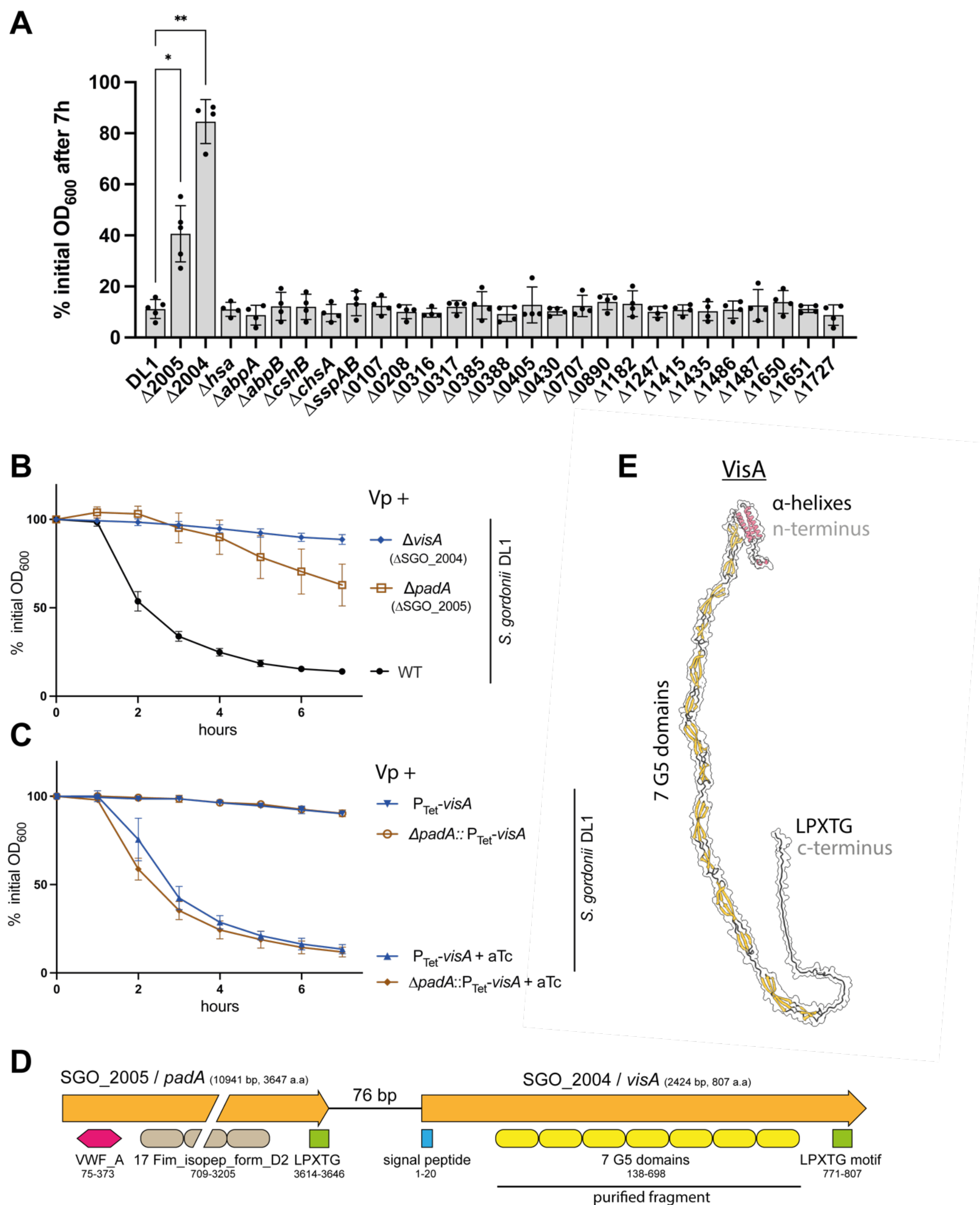

287

288 **Figure 2: VisA (SGO_2004) is a novel adhesin interacting with *V. parvula.***

289 (A) Co-aggregation of *V. parvula* SKV38 with *S. gordonii* DL1 WT and mutants for each LPXTG-con-
290 taining protein and *abpA-B*, as measured by the % of decrease of optical density between 0 and 7h. SD

bioRxiv preprint doi: https://doi.org/10.1101/2024.07.16.603716; this version posted July 16, 2024. The copyright holder for this preprint (which was not certified by peer review) is the author/funder, who has granted bioRxiv a license to display the preprint in perpetuity. It is made available under aCC-BY-NC-ND 4.0 International license.

291 and single points for 4-5 replicates are shown. The indicated p-values were calculated by comparing all
292 conditions to the partner + *Vp* WT using a Brown-Forsythe and Welch ANOVA followed by Dunnett
293 correction. Co-aggregation curves of *S. gordonii* WT, Δ*visA,* Δ*padA* (B) and P_{Tet}-*visA* or P_{Tet}-*padA* (C)
294 with or without 250 ng aTc. Curves represent the mean and SD of 6-13 replicates. (D) Genetic organi-
295 zation of the SGO_2004/2005 locus. VWF_A: Von Willbrand factor A (IPR002035), Fim_iso-
296 pep_form_D2: Fimbrial isopeptide formation D2 domain (IPR026466), G5 domain (IPR011098). (E) Al-
297 phaFold structural model of VisA without the signal peptide.

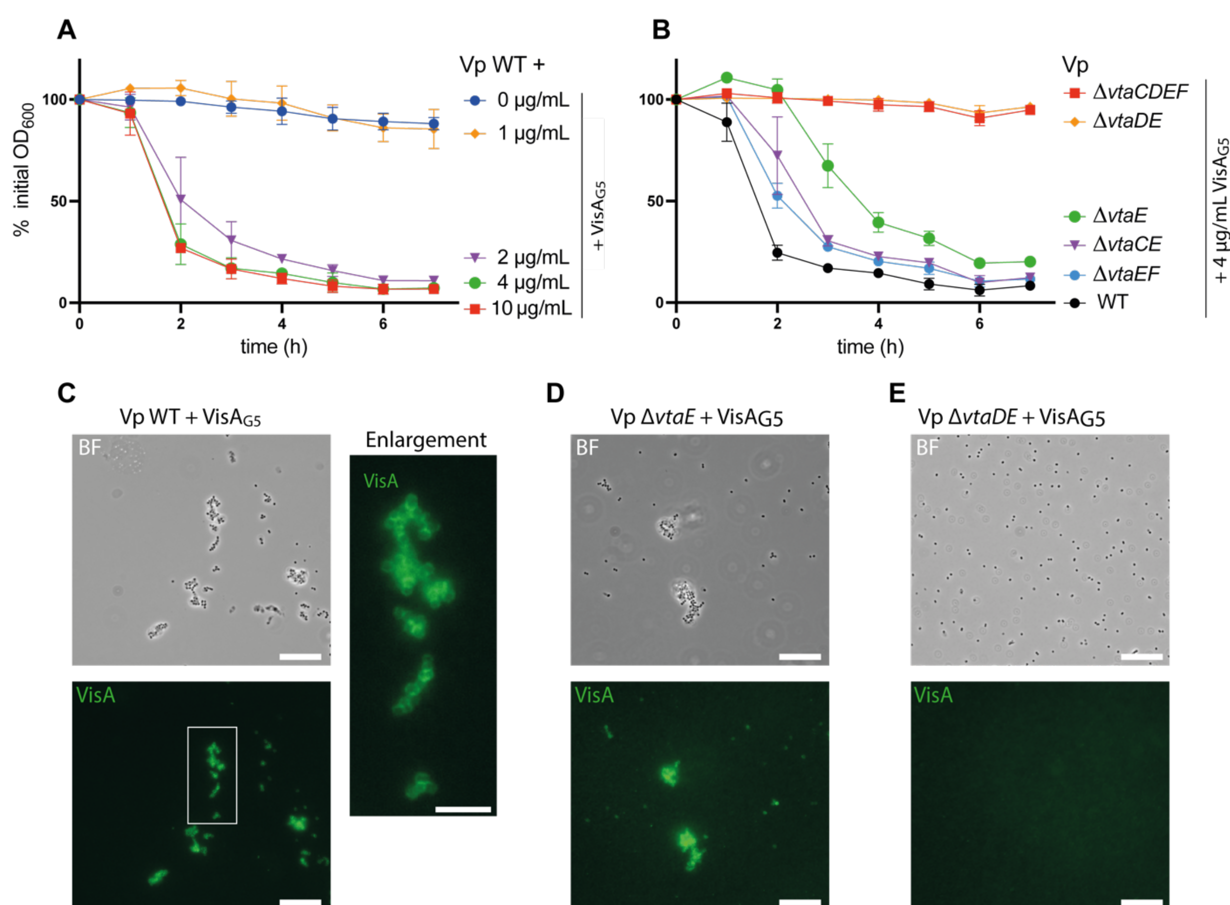

298

299 **Figure 3: VisA binds directly to *V. parvula* by interacting with VtaE and VtaD.**

300 (A) Auto-aggregation curves of *V. parvula* SKV38 with various concentrations of $VisA_{G5}$. (B) Aggregation
301 curve of *V. parvula* SKV38 or indicated adhesin mutants with 4 µg/mL of $VisA_{G5}$. For (A) and (B), curves
302 represent the mean and SD of 3 replicates. (C-E) Brightfield images and their corresponding immuno-
303 fluorescence images targeting the His-tag of $VisA_{G5}$ after incubation of *Vp* WT, Δ*vtaE* and Δ*vtaDE* with
304 10 µg/mL of $VisA_{G5}$ protein. Scale bar is 15 µm. The (C) right panel represents an enlargement of WT +
305 $VisA_{G5}$ immunofluorescence image (indicated by the white square) and scale bar is 5 µm.
306
307
308

309 Co-aggregation in co-culture produces no significant alteration on the 310 transcriptomic profiles of *V. parvula* and *S. gordonii*

311

bioRxiv preprint doi: https://doi.org/10.1101/2024.07.16.603716; this version posted July 16, 2024. The copyright holder for this preprint (which was not certified by peer review) is the author/funder, who has granted bioRxiv a license to display the preprint in perpetuity. It is made available under aCC-BY-NC-ND 4.0 International license.

312 While previous studies have compared the transcriptional responses of
313 *Veillonella* and *S. gordonii* co-incubations compared to monoincubation[18,19,29], they did
314 not specifically evaluate the potential contribution of co-aggregation. Having identified
315 the adhesins involved in *V. parvula / S. gordonii* co-aggregation, we set out to compare
316 the transcriptional responses of these two strains in mono- and cocultures with and
317 without co-aggregation or auto-aggregation. Here we used the rich medium BHIP (BHI
318 + 100 mM pyruvate), in which both bacteria could grow without metabolic co-
319 dependency.
320
321 *V. parvula* transcriptional profiles of each condition grouped mainly by the
322 presence of *S. gordonii* and then by their strain type. In principal component analysis
323 (PCA), calculated using normalized transcripts counts, samples were strongly
324 separated on the first principal component by their coculture status, thus indicating that
325 the main determinant of the observed *V. parvula* response is the presence of its
326 bacterial partner *S. gordonii* (Figure 4A). The PCA analysis on the second and third
327 axis revealed a clustering by *V. parvula* mutant (Figure S8), suggesting that the
328 residual differences between conditions are associated with the nature of the *V. parvula*
329 mutants.
330 In order to identify potential coculture-specific response, we searched for genes
331 up or downregulated (log2Fold above 1 or below -1) in at least one condition compared
332 to *V. parvula* WT monocultures. The resulting Upset plot (Figure 4B) represents the
333 common dysregulated genes for different combinations of conditions. This plot shows
334 that the core *V. parvula* coculture transcriptomic response in all conditions was
335 composed of 68 genes (Figure 4B green bar and supplementary data S1). The most
336 upregulated gene was *FNLLGLLA_00352* (around 4.5 log2Fold increase compared to
337 the monoculture), coding for an uncharacterized major facilitator superfamily-type
338 (MFS) transporter, an inner membrane transporter of an unknown small molecule. We
339 also found a strong upregulation of genes coding for enzymes of the histidine and
340 arginine biosynthesis pathways (Figure 4C). Interestingly, *vtaB*, encoding an
341 uncharacterized trimeric autotransporter and a gene cluster encoding a prophage were
342 also induced, albeit at lower levels. Many genes associated with stress response were
343 slightly upregulated (genes coding for the chaperones GroEL and GroES, their
344 regulators CtsR and HcrA, ClpC and ClpE) (supplementary data S1). Pyruvate

bioRxiv preprint doi: https://doi.org/10.1101/2024.07.16.603716; this version posted July 16, 2024. The copyright holder for this preprint (which was not certified by peer review) is the author/funder, who has granted bioRxiv a license to display the preprint in perpetuity. It is made available under aCC-BY-NC-ND 4.0 International license.

345 metabolism appeared to be remodeled in coculture by up- and downregulation of many
346 pyruvate-associated genes (Figure 4C, supplementary data S1). Concerning lactate
347 consumption, the malate/lactate antiporter *mleN* was slightly up-regulated, while genes
348 related to the L- and D-lactate dehydrogenases were downregulated (*lutA*-*lutC*,
349 *FNLLGLLA_01898* and *fucO*). Genes involved in iron or other metal uptake through
350 the inner membrane were also both up- and downregulated.
351 We also compared specifically all coculture conditions compared to *V. parvula*
352 Δ*vtaADE* with *S. gordonii* (Figure 4D). Overall, only a few *V. parvula* genes involved in
353 purine metabolism were upregulated specifically wen aggregating in cocultures, either
354 through co-aggregation or auto-aggregation (Figure 4B and D, blue bar, supplementary
355 data S1). By contrast, 22 genes were specifically dysregulated in coculture in absence
356 of any type of aggregation among which genes involved in NADH regeneration through
357 xanthine to urate conversion were slightly downregulated (Figure 4B, orange bar,
358 supplementary data S1).
359
360 On the other hand, there were very few changes on *S. gordonii* transcriptome
361 when cocultured with *V. parvula*. The only upregulated genes in all cocultures
362 conditions (Figure 5AB, green bar, supplementary data S2) are part of the Bfb PTS
363 system (SGO_1575-82) already described as induced when co-aggregating with *A.*
364 *naeslundii*[30]. The only downregulated gene (SGO_1314) encoded a ZnuA-like metal
365 binding lipoprotein (Figure 5C). No gene expression changes were found specifically
366 associated to co-aggregation (Figure 5D).
367 Altogether, these results indicate that (i), *V. parvula* transcriptional response to
368 coculture is associated with changes in metabolism and stress (ii) *S. gordonii* has a
369 minimal transcriptional response, (iii) . aggregation has only a limited effect on both
370 bacteria, without contribution of auto- or co-aggregation.
371
372

bioRxiv preprint doi: https://doi.org/10.1101/2024.07.16.603716; this version posted July 16, 2024. The copyright holder for this preprint (which was not certified by peer review) is the author/funder, who has granted bioRxiv a license to display the preprint in perpetuity. It is made available under aCC-BY-NC-ND 4.0 International license.

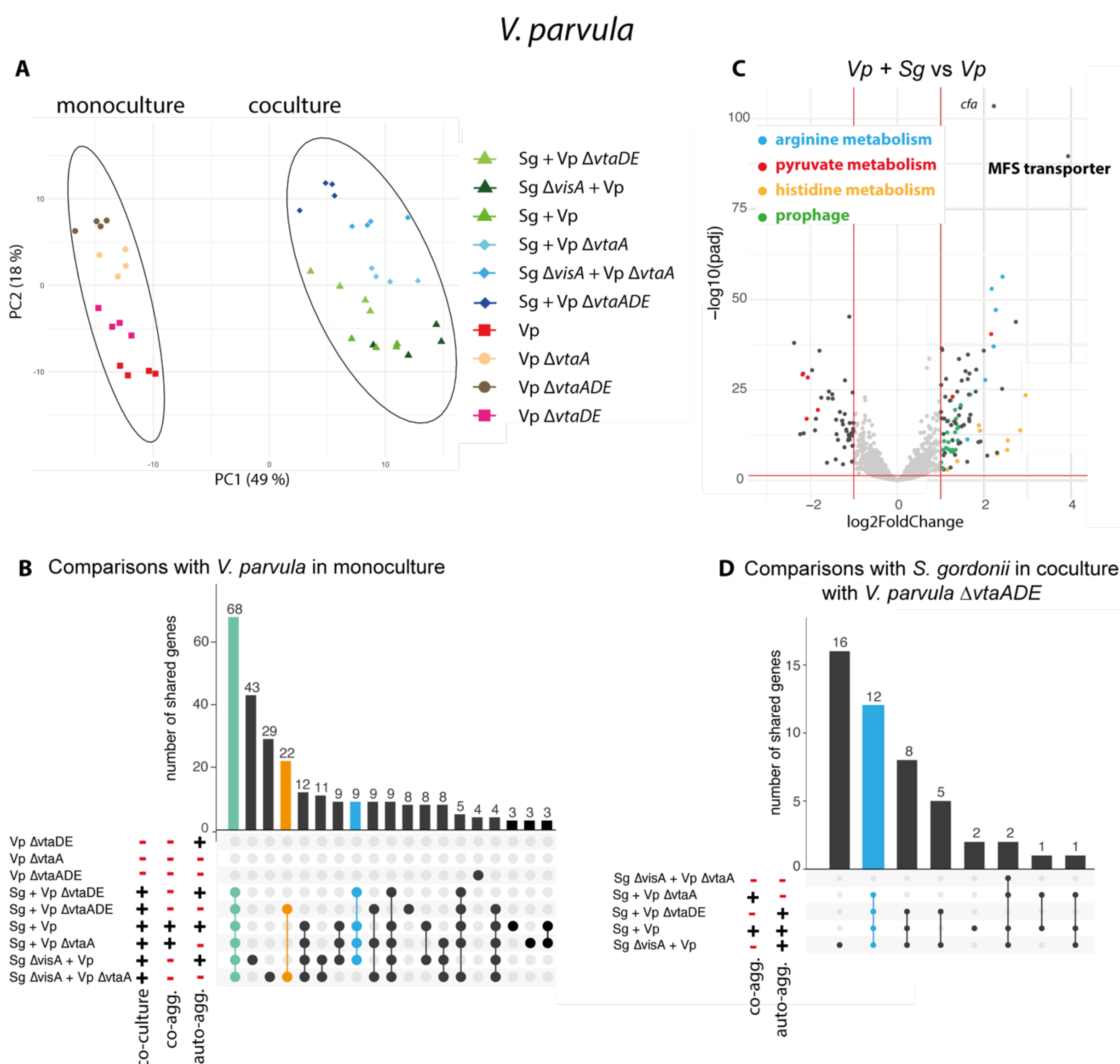

373

374 **Figure 4: Transcriptomic response of *V. parvula* to *S. gordonii* is mostly related**

375 **to coculture.**

376 A) Principal component analysis (PCA) of all *V. parvula* samples (4 biological replicates for 10
377 conditions). Colors and shape represent the different conditions. The two circles separate monoculture
378 samples from coculture samples. Green symbols indicate samples able to auto-aggregate in coculture,
379 blue shades samples unable to auto-aggregate. B) Upset plot (a Venn diagram alternative) showing the
380 number of differentially expressed genes (defined by an absolute log2fold change > 1) shared for each
381 condition compared to *V. parvula* WT monoculture. The green bar indicates the core response to
382 coculture, the orange bar the core answer to coculture without any aggregation and the blue bar the
383 response to any aggregation in coculture. C) Volcano plot of the coculture of *V. parvula* and *S. gordonii*
384 WT compared to *V. parvula* in monoculture. Genes corresponding to identified key functions are
385 differentially colored. D) Upset plot for each condition compared to *V. parvula* ΔvtaAΔvtaDE and *S.*
386 *gordonii* coculture., the blue bar shows the response to any aggregation in coculture.

387

388

bioRxiv preprint doi: https://doi.org/10.1101/2024.07.16.603716; this version posted July 16, 2024. The copyright holder for this preprint (which was not certified by peer review) is the author/funder, who has granted bioRxiv a license to display the preprint in perpetuity. It is made available under aCC-BY-NC-ND 4.0 International license.

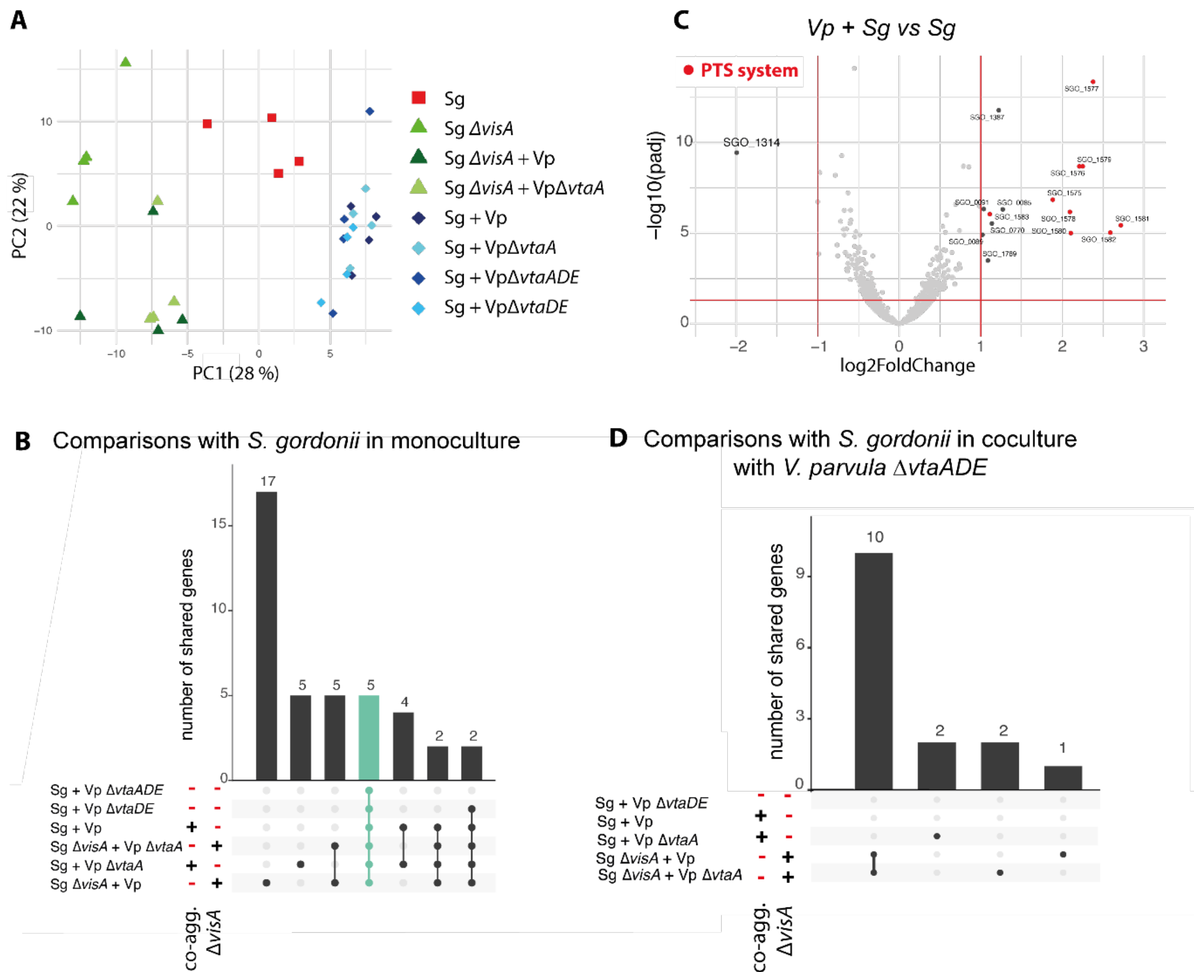

Figure 5: Transcriptomic response of *S. gordonii* to *V. parvula* is limited to the upregulation of a PTS system and downregulation of a metal binding lipoprotein. A) Principal component analysis (PCA) of all *S. gordonii* samples (4 biological replicates for 10 conditions). Shades of green represent all *S. gordonii* ΔvisA conditions, shades of blue cocultures of *S. gordonii* WT and red the monoculture of *S. gordonii* WT. B) Upset plot (Venn diagram alternative) showing the number of differentially expressed genes (defined by an absolute log2fold change > 1) shared for each condition compared to *S. gordonii* WT or Δ*visA* monocultures (indicated by the Δ*visA* column). The green bar indicates the core response to coculture and the blue bar the core differences between *S. gordonii* WT and Δ*visA*. C) Volcano plot of the coculture of *V. parvula* and *S. gordonii* WT compared to *S. gordonii* in monoculture. Genes of the PTS system are colored in red. D) Upset plot for each coculture condition compared to *S. gordonii* + *V. parvula* Δ*vtaA*Δ*vtaDE* coculture.

bioRxiv preprint doi: https://doi.org/10.1101/2024.07.16.603716; this version posted July 16, 2024. The copyright holder for this preprint (which was not certified by peer review) is the author/funder, who has granted bioRxiv a license to display the preprint in perpetuity. It is made available under aCC-BY-NC-ND 4.0 International license.

411 **Co-aggregation strongly affects the structure of mixed *V. parvula*/*S. gordonii***
412 **biofilms.**
413
414 To assess the impact of co-aggregation on mixed biofilm formation, we imaged
415 either mono-species or mixed biofilms of *V. parvula* and *S. gordonii* formed in 96 well
416 plates for 24h using confocal laser scanning microscopy (CLSM). To differentiate both
417 bacteria, *S. gordonii* was stained using the monoderm specific dye BacGO[31] while
418 Syto61 was used to stain all bacterial (Figure S9A-B). Comparison of co-aggregating
419 mixed biofilms (*Vp* WT + *Sg* WT) with mixed biofilms without co-aggregation (*Vp*
420 Δ*vtaDE* + *Sg* Δ*visA*, *Vp* Δ*vtaDE* + *Sg* WT and *Vp* WT +*Sg* Δ*visA*) showed that, in
421 absence of co-aggregation, the two partner bacteria were found in distinct patches
422 (Figure 6A). This was confirmed by the measurement of roughness (capturing the
423 variations of height over the biofilm) of the streptococcus biofilm in mixed biofilms
424 (Figure 6B, figure S9C-D). However, co-aggregating biofilms presented a more
425 homogenous distribution of the two bacterial populations (Figure 6A). Volume
426 measurements were variable but suggested that co-aggregation results in a higher
427 overall biofilm volume and an increased *S. gordonii* biofilm (Figure S9E-F). Measures
428 of total biofilm formation by crystal violet assay did not show an increase in biofilm
429 formation when co-aggregating (Figure S9G). Coaggregation therefore seems to
430 strongly impact on the organization of the two species in mixed biofilms which could
431 profoundly modulate the behavior of these species *in vivo*.

bioRxiv preprint doi: https://doi.org/10.1101/2024.07.16.603716; this version posted July 16, 2024. The copyright holder for this preprint (which was not certified by peer review) is the author/funder, who has granted bioRxiv a license to display the preprint in perpetuity. It is made available under aCC-BY-NC-ND 4.0 International license.

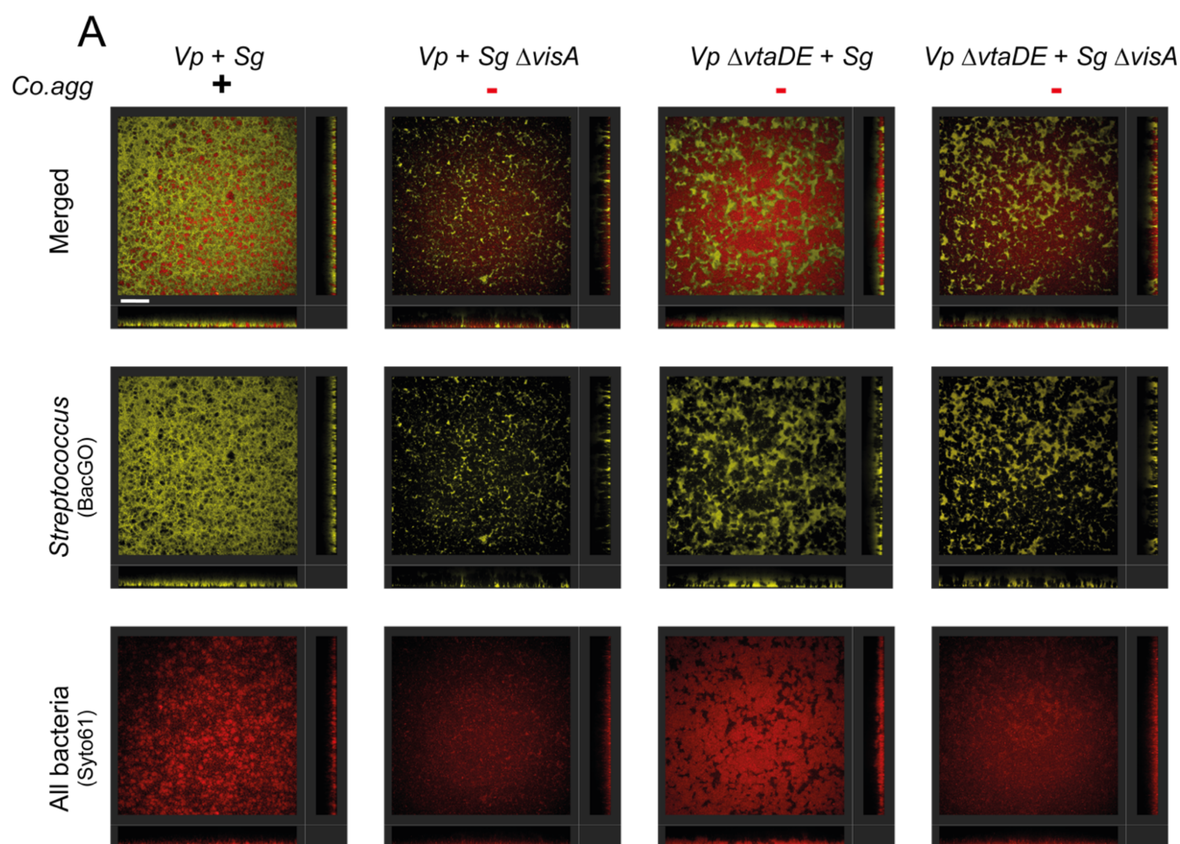

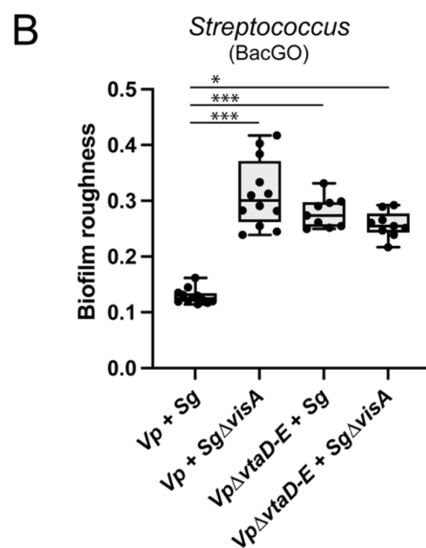

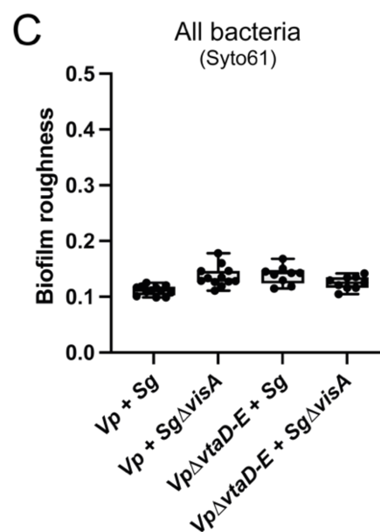

432
433
434 **Figure 6: Confocal microscopy of mixed biofilms.** A) Representative section images of
435 mixed biofilms, scale bar is 60 µm. Lower and side bands correspond to the orthogonal projections
436 on the z-x and z-y axis respectively. B-C) Measured biofilm roughness parameter for the BacGO
437 and the Syto61 dyes. Each point (9-12 per condition) represents the average roughness
438 measurement of four images per well. Experiment done in three biological independent replicates
439 and three technical replicates. P-values, indicated by asterisk (*: p< 0,05, *** : p< 0,0005) were
440 calculated using a Kruskal-Wallis test with Dunn's correction for multiple testing. For all plots, *Vp* is
441 *V. parvula*, ΔDE is *V. parvula ΔvtaD-vtaE*, *Sg* is *S. gordonii* and Δ*visA* is *S. gordonii* Δ*visA*. Presence
442 (or absence) of auto- and co- aggregation is indicated by the + (or -) symbols.
443
444

bioRxiv preprint doi: https://doi.org/10.1101/2024.07.16.603716; this version posted July 16, 2024. The copyright holder for this preprint (which was not certified by peer review) is the author/funder, who has granted bioRxiv a license to display the preprint in perpetuity. It is made available under aCC-BY-NC-ND 4.0 International license.

445 **DISCUSSION**

446

447 Interactions between bacteria and their environment, whether abiotic or biotic,
448 play a key role in determining the nature and evolution of bacterial lifestyles and we
449 previously characterized the *V. parvula* adhesins involved in its biofilm formation
450 capacities. In this study, we investigated the molecular determinants at the origin of the
451 co-aggregation mechanisms between *V. parvula* and different members of the dental
452 plaque and identified three *V. parvula* and one new *S. gordonii* adhesins involved in
453 co-aggregation and studied the impact of such co-aggregation on partner physiology
454 and co-biofilm structure.

455

456 **Adhesion strategies in *Veillonella***

457 We showed that the previously identified *V. parvula* VtaA adhesin interacts with
458 *S. oralis* and *A. oris* while VtaE is responsible for co-aggregation with *A. oris* and *S.*
459 *gordonii*, in which the highly homologous, but truncated VtaD has a secondary
460 contribution (Figure 7).

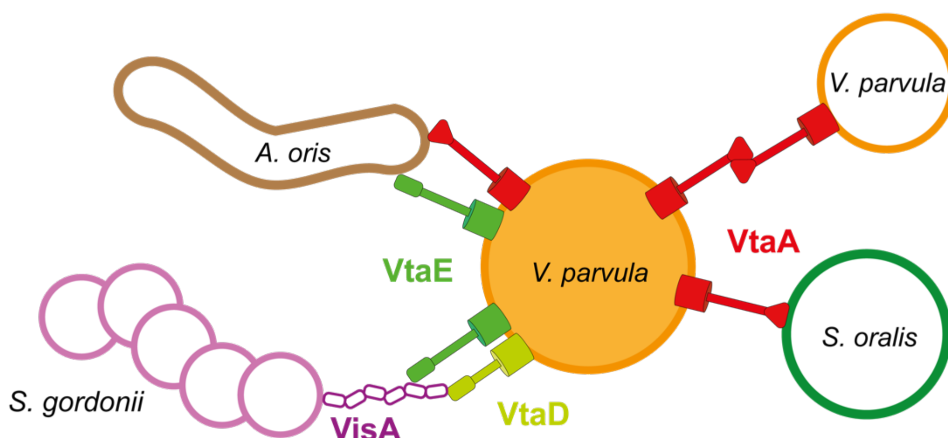

461

462 **Figure 7: The multiple roles of *V. parvula* adhesins.**

463 Model of the interactions mediated by the different *V. parvula* adhesins.

464

465 Contrary to what has been described for *V. atypica*, where a single adhesin,
466 Hag1, is responsible for all aggregative phenotypes[23], the different adhesive functions
467 in *V. parvula* are located on different proteins. Comparison of the predicted structures
468 of Hag1 with VtaE, VtaD and VtaA shows that Hag1 head section is much more
469 developed than the other adhesins, which could explain its pleiotropic role (Figure
470 S3B). In addition, Hag1 is almost twice the size in residues (7187 residues) compared

bioRxiv preprint doi: https://doi.org/10.1101/2024.07.16.603716; this version posted July 16, 2024. The copyright holder for this preprint (which was not certified by peer review) is the author/funder, who has granted bioRxiv a license to display the preprint in perpetuity. It is made available under aCC-BY-NC-ND 4.0 International license.

471 to Hag2 (3838 residues), the second longest adhesin in *V. atypica* OK5. In *V. parvula*
472 SKV38, all major adhesins, including VtaA (3041 residues), VtaE (3142 residues),
473 VtaC (2811 residues) and VtaF (3193 residues) are of similar size. One hypothesis is
474 that Hag1, because of its long size, could mask other adhesins at the cell surface thus
475 explaining the concentration of activities on the only surface accessible adhesin. By
476 contrast, in *V. parvula* SKV38, activities are distributed across multiple co-expressed
477 surface adhesins. VtaD and VtaE head domains are very similar, but VtaE is estimated
478 to be around 100 nm longer than VtaD (Figure S3A) and we observed that more
479 discrete aggregative phenotypes are associated with VtaD compared to VtaE, which
480 could be due to masking of VtaD by VtaE. Additionally, the fact that the double mutants
481 Δ*vtaE*Δ*vtaF* and Δ*vtaE*Δ*vtaC* aggregate faster with the purified *S. gordonii* $VisA_{G5}$ than
482 the simple Δ*vtaE* mutant is also in favor of the hypothesis that a shorter VtaD adhesin
483 is partially masked by the longer VtaC and VtaF adhesins. This masking interference
484 between adhesins has been commonly observed as a possible regulatory mechanism
485 of the surface structures [15–16]. Therefore, selection pressure on adhesion could either
486 apply towards ensuring that the main adhesins do not mask each other by remaining
487 of similar size, still allowing some potential interference relief of shorter adhesins (*V.*
488 *parvula* case) or towards accumulating all functions on the tallest adhesin (*V. atypica*
489 case).

490 Here we identified VtaA as an adhesin promoting co-aggregation with *S. oralis*,
491 whereas we previously showed that VtaAit promotes auto-aggregation in BHI[34]. This
492 auto-aggregation does not happen after growth in SK medium, which was used to grow
493 *V. parvula* for co-aggregation assays. This switch from an auto-aggregative to a co-
494 aggregative behavior depends on environmental conditions. This could be an efficient
495 mean to rapidly adapt to abrupt changes of environment without affecting the quantity
496 of a single adhesin at the cell surface.

497 Different *Veillonella* species occupy different niches within the oral microbiome.
498 *V. parvula* is strongly associated with the dental plaque while *V. atypica* and *V. dispar*
499 are found on soft surfaces. *Veillonella* HMT 780 has a strong specialization for
500 keratinized gingiva[16]. It would be interesting to know if differential colonization sites
501 stem from different co-aggregation capacities. This site specialization has been
502 associated to certain genes (e.g., thiamine biosynthesis genes) but no difference in
503 the number of adhesins between sites could be seen[16]. However, older studies have

bioRxiv preprint doi: https://doi.org/10.1101/2024.07.16.603716; this version posted July 16, 2024. The copyright holder for this preprint (which was not certified by peer review) is the author/funder, who has granted bioRxiv a license to display the preprint in perpetuity. It is made available under aCC-BY-NC-ND 4.0 International license.

504 shown that *Veillonella* isolates from different origin within the mouth presented site
505 specific co-aggregation capacities[7]. Revisiting the concept of strain-specific co-
506 aggregation with a modern genetic approach leveraging genome sequencing and
507 genetic manipulation, could help us decipher whether *Veillonella* adhesins specificity
508 to different bacteria is related to the site specificity.
509 We found that *V. parvula* binds weakly to human epithelial cells. This differs to
510 what has been described in *V. atypica*[23]. Therefore, different species of *Veillonella*
511 might show different adhesion capacity to host cells, maybe linked to their isolation
512 niche or their adhesin repertoire. We cannot discount that technical differences in our
513 assay explain that difference. We used cancer cell lines, whereas Zhou *et al.* used
514 buccal cells from a human buccal swab. In addition, the buccal cells were not
515 thoroughly washed after adhesion as in our present protocol.
516
517 **VisA, a novel adhesin of *S. gordonii***
518 Like *V. parvula, S. gordonii* DL1 seems to use different adhesins to bind to
519 different partners. For instance, it binds to certain *Veillonella* species, including *V.*
520 *atypica* OK5, through Hsa, a sialic-acid binding protein also involved in platelet
521 activation[24,32,33]. Here, we showed that Hsa is not involved in *S. gordonii* co-
522 aggregation with *V. parvula* SKV38 (Figure 2A) and we have identified a second and
523 new adhesin, VisA (SGO_2004), responsible for this interaction. Our results also
524 suggest that VisA interacts directly with VtaE and VtaD. The use of purified VisA G5
525 domains demonstrated that they are the portion of VisA recognized by *V. parvula*. G5
526 domains are structural folds that are part of the stalk of monoderm surface proteins
527 and are often found associated to an enzymatic active site[35]. For instance, SasG from
528 *Staphylococcus aureus* or Aap from *Staphylococcus epidermidis* promote auto-
529 aggregation through interaction between the G5-E domain repeats forming their B
530 domain and have been described to undergo a zinc mediated dimerization[36]. While
531 VisA does not seem to induce auto-aggregation of *S. gordonii*, the purified protein
532 migrated exclusively at a size corresponding to a dimer in denaturing western blot
533 (something also observed for trimeric autotransporters), suggesting that it also
534 possesses the ability to dimerize even without the E-linker domain (Figure S10).
535

bioRxiv preprint doi: https://doi.org/10.1101/2024.07.16.603716; this version posted July 16, 2024. The copyright holder for this preprint (which was not certified by peer review) is the author/funder, who has granted bioRxiv a license to display the preprint in perpetuity. It is made available under aCC-BY-NC-ND 4.0 International license.

536 Interestingly, the locus encompassing genes encoding VisA-like proteins, PadA
537 and a thioredoxin reductase is conserved in distant pathogenic *Streptococci* (Figure
538 S7). PadA, in interaction with Hsa, is known to bind to platelets triggering their activa-
539 tion[33]. While in laboratory condition VisA (formerly known as SGO_2004) does not play
540 a role in platelet interaction[27], its conservation could suggest otherwise *in vivo*. *S. oralis*
541 ATCC 10557 also possesses homologues of PadA (HRJ33_07090) and VisA
542 (HRJ33_07095). However, *V. parvula* adhesins responsible for co-aggregation with
543 the *S. gordonii* and *S. oralis* species are not the same, which strongly indicates that *S.*
544 *oralis* likely uses a protein different from VisA to co-aggregate with *V. parvula*. The *S.*
545 *oralis* VisA homologue possesses only five G5 domains while *S. gordonii* VisA has
546 seven domains. The protein could be too short in *S. oralis* and masked by other surface
547 components or not expressed. This could explain that VisA does not contribute to *S.*
548 *oralis* co-aggregation with *V. parvula*.
549 Taken together, these results further illustrate the versality in the use of various
550 adhesins to co-aggregate both for Streptococci and Veillonella species.
551
552 **What drives the response to coculture in oral bacteria?**
553 Although limited, modifications of gene expression during coculture of *V. parvula*
554 and *S. gordonii* were observed. For *S. gordonii*, the main answer to coculture with *V.*
555 *parvula* was the upregulation of a PTS system encoded by the *bfb* operon (SGO_1575-
556 1582). This system was found upregulated in *S. gordonii* when co-aggregating with
557 *Actinomyces oris*[30] and one gene of the operon downregulated when co-aggregating
558 with *Fusobacterium nucleatum*[37]. The *bfb* operon is associated with biofilm formation
559 as deletion of several genes led to a decrease in adhesion and biofilm formation while
560 the operon promoter was 25% more active in biofilms[38]. An increase of arginine
561 concentration could be at the origin of the induction of this *S. gordonii* PTS system.
562 Indeed, arginine is known to be important for *S. gordonii* biofilm formation and arginine
563 restrictions result in strong downregulation of the *bfb* operon in monoculture[39]. Co-
564 aggregation of *S. gordonii* with *A. oris* resulted in downregulation of arginine
565 biosynthesis and upregulation of the *bfb* operon through the uptake of *A. oris* -produced
566 arginine. One of the upregulated pathways in *Veillonella* when cocultured with *S.*
567 *gordonii* is arginine biosynthesis. Therefore, one can hypothesize that *V. parvula* would
568 favor *S. gordonii* biofilm formation by producing arginine. We have, however, not

bioRxiv preprint doi: https://doi.org/10.1101/2024.07.16.603716; this version posted July 16, 2024. The copyright holder for this preprint (which was not certified by peer review) is the author/funder, who has granted bioRxiv a license to display the preprint in perpetuity. It is made available under aCC-BY-NC-ND 4.0 International license.

569 detected any decrease in the arginine biosynthesis pathway in *S. gordonii* or changes
570 in expression of arginine dependent regulators *argC, argR* or *argC*.
571 Globally, coculture did not result in major changes in gene expression in our
572 experiments performed in anaerobic conditions using a rich and buffered media without
573 metabolic dependency. Auto-aggregation and co-aggregation themselves had a
574 negligible impact on the observed responses by both bacteria. The induction of the
575 alpha-amylase *amyB* gene expression in *S. gordonii* caused by a an unknown diffusible
576 signal produced by *V. parvula*[18,19] was not observed in our experiments. This may be
577 due to our specific conditions that did not allow production of the signal by *V. parvula*.
578 Other examples of oral bacteria responding weakly to co-aggregation are *F. nucleatum*
579 interacting with *S. gordonii*[37] and *S. mutans* interacting with *V. parvula*[40,41]. These
580 results suggest that oral bacteria do not actually sense attachment to other bacteria
581 but rather changes in nutrient availability and environment conditions such as pH or
582 oxidative stress. Auto-aggregation and biofilm lifestyle is known to induce large
583 metabolic changes in common aerobic bacteria, inducing genes involved in stress
584 response and anaerobic metabolism in *E. coli*[42] which seem mostly driven by oxygen
585 gradients, as shown in aggregates of *P. aeruginosa* [43].
586 While anaerobic conditions could explain the limited response caused during
587 coculture and interactions between *V. parvula* and *S. gordonii*, the exposure to oxygen
588 could strongly impact the response to co-aggregation of anaerobic bacteria. Indeed, in
589 another study looking at *S. gordonii and V. parvula* co-transcriptomes, Mutha *et al.*
590 reported broad changes in *Veillonella* including a predominant response to oxidative
591 stress with 39 out of 272 regulated genes associated with it while *S. gordonii* samples
592 presented high inter-variability[29]. No common gene regulation could be detected
593 between our results and their results, possibly due to different experimental settings,
594 as they looked at response from short (30 min) aerobic co-aggregation in saliva while
595 we looked at transcriptional responses after 6 h of anaerobic coculture. The aerobic
596 conditions used during this short co-aggregation period could explain the strong *V.*
597 *parvula* response to oxidative stress exacerbated by *S. gordonii.*
598
599
600

bioRxiv preprint doi: https://doi.org/10.1101/2024.07.16.603716; this version posted July 16, 2024. The copyright holder for this preprint (which was not certified by peer review) is the author/funder, who has granted bioRxiv a license to display the preprint in perpetuity. It is made available under aCC-BY-NC-ND 4.0 International license.

601 **Could the proximity within the biofilm enhance synergistic or antagonistic**
602 **interactions?**
603 We hypothesized that co-aggregation could influence localization of the two
604 bacteria within the biofilm. Indeed, co-aggregation was necessary to promote
605 colocalization of the two bacteria. Proximity within the biofilm would be essential to
606 *Veillonella parvula* as it can favor the uptake of lactate by bringing it closer to the
607 producer Streptococci, which would also protect it from oxidative stress by consuming
608 the O_2 locally. It could also favor signal transduction as demonstrated for the distance
609 dependent induction of *S. gordonii amyB*.
610 Without co-aggregation, both bacteria were distant from each other in the
611 biofilm. This could be explained by a passive clonal development but also by an active
612 prevention of biofilm colonization by non-aggregating partners. This could have a
613 strong effect *in vivo* by limiting the entry of non-co-aggregating members (including *S.*
614 *mutans*) into the dental plaque biofilm while permitting the presence of cooperative
615 partners in close vicinity. A similar mechanism has been demonstrated in *Vibrio*
616 *cholerae*, where deletion of *rbmA*, the gene encoding RbmA, a matrix protein involved
617 in mother-daughter cell cohesion, resulted in higher penetration by invaders as cells
618 were less tightly packed in the biofilm[44]. Additionally, mixed biofilms between RbmA
619 producers and deficient strains resulted in patchy structures reminiscent of our
620 observation.
621 Mixed biofilms have often been described to increase stress resistance
622 compared to single species biofilms. For instance, synergistic biofilm formation by four
623 marine bacteria promoted protection to invasion by the pathogen *Pseudoalteromonas*
624 *tunicata* and increased resistance to hydrogen peroxide and tetracycline compared to
625 monospecies biofilms[45]. The resistance in a three-species biofilm was due to
626 protective capacity of one of the resident members[46]. We hypothesize that, while mixed
627 biofilms are already more stress-resistant, co-aggregation between members could
628 further increase stress resistance.
629
630 In conclusion, we have shown that *V. parvula* uses specific sets of multiple
631 trimeric autotransporters to specifically interact with other members of the oral dental
632 plaque. While these adhesive capacities are not necessary for intercellular
633 communication, they reduce distance between members of the biofilm. The co-

bioRxiv preprint doi: https://doi.org/10.1101/2024.07.16.603716; this version posted July 16, 2024. The copyright holder for this preprint (which was not certified by peer review) is the author/funder, who has granted bioRxiv a license to display the preprint in perpetuity. It is made available under aCC-BY-NC-ND 4.0 International license.

634 aggregation phenomena are likely to contribute to the highly organized process of
635 dental plaque formation by modulating the successive addition of interacting bacterial
636 species.
637

638 MATERIAL AND METHODS

639

640 Growth conditions

641 Bacterial strains are listed in TABLE S1. *Streptococcus* spp. and *A. oris* were
642 grown in brain heart infusion (BHI) medium (Bacto brain heart infusion; Difco*). V. par-*
643 *vula* was grown in BHI supplemented with 0.6% sodium dl-lactate (BHIL) or SK me-
644 dium (10 g liter−1 tryptone [Difco], 10 g liter−1 yeast extract [Difco], 0.4 g liter−1 diso-
645 dium phosphate, 2 g liter−1 sodium chloride, and 10 ml liter−1 60% [wt/vol] sodium dl-
646 lactate; described in Knapp et al.[47]), in which it does not auto-aggregate. Bacteria were
647 incubated at 37°C under anaerobic conditions in anaerobic bags (GENbag anaero;
648 bioMérieux no. 45534) or in a C400M Ruskinn anaerobic-microaerophilic station. *Esch-*
649 *erichia coli* was grown in lysogeny broth (LB) (Corning) medium under aerobic condi-
650 tions at 37°C. When needed, 20 mg/L chloramphenicol (Cm), 200 mg/L erythromycin
651 (Ery), 300 mg kanamycin (Kan) or 2.5 mg/L tetracycline (Tet) was added to *V. par-*
652 *vula* cultures, 5 mg/L Ery was added to *S. gordonii* cultures and 25 mg/L Cm or
653 100 mg/L ampicilin (Amp) was added to *E. coli* cultures. All chemicals were purchased
654 from Sigma-Aldrich unless stated otherwise.
655

656 *Veillonella parvula* natural transformation

657 From plate, cells were resuspended in 1 mL SK medium adjusted to an optical
658 density at 600 nm (OD_{600}) of 0.4 to 0.8, and 15 µL was spotted on SK agar petri dishes.
659 On each drop, 1-5 µL (75 to 200 ng) linear double-stranded DNA PCR product was
660 added. The plates were then incubated anaerobically for 24-48 h. The biomass was
661 resuspended in 500 µL SK medium, plated on SK agar supplemented with the corre-
662 sponding antibiotic, and incubated for another 48 h. Colonies were streaked on fresh
663 selective plates, and the correct integration of the construct was confirmed by PCR
664 and sequencing.
665

bioRxiv preprint doi: https://doi.org/10.1101/2024.07.16.603716; this version posted July 16, 2024. The copyright holder for this preprint (which was not certified by peer review) is the author/funder, who has granted bioRxiv a license to display the preprint in perpetuity. It is made available under aCC-BY-NC-ND 4.0 International license.

666 ***Veillonella parvula* mutagenesis and complementation.**

667 *V. parvula* site directed mutagenesis was performed as described by Knapp and
668 al[47] and Béchon et al[25]. Briefly, upstream and downstream homology regions of the
669 target sequence and the *V. atypica* kanamycin (*aphA3* derived from the pTCV-erm[48]
670 plasmid under the *V. parvula* PK1910 *gyrA* promoter) or tetracycline resistance cas-
671 sette were PCR amplified with overlapping primers using Phusion Flash high-fidelity
672 PCR master mix (Thermo Scientific, F548). PCR products were used as templates in
673 a second PCR round using only the external primers, resulting in a linear dsDNA with
674 the antibiotic resistance cassette flanked by the upstream and downstream sequences.
675 *vtaE* chromosomal complementation was done by inserting in the promoter region the
676 previously described *Veillonella* P_{Tet} promoter[25] associated with an erythromycin re-
677 sistance cassette. Primers used in this study are listed in Table S2 in the supplemental
678 material.

679

680 ***Streptococcus gordonii* natural transformation**

681 25 µL of an O/N culture, 100 µL of heat inactivated horse serum (Sigma), 900
682 µL of THY Broth, 2 µL of competence specific peptide (1 mg/mL,
683 DLRGVPNPWGWIFGR, synthetized by GenScript) and 1-5 µL of linear double-
684 stranded DNA PCR product were mixed in a microcentrifuge tube, incubated anaero-
685 bically for 5 to 8 hours at 37°C and plated on selective agar medium for 1 to 3 days.
686 Colonies were streaked on fresh selective plates, and the correct integration of the
687 construct was confirmed by PCR and sequencing.

688

689 ***Streptococcus gordonii* complementation.**

690 In order to create a markerless mutant of *SGO_2004* with a P_{Tet} promoter, we
691 took advantage of the described IDFC2 cassette[49], containing an erythromycin re-
692 sistance and a mutant *pheS* gene encoding the A314G missense mutation providing
693 sensitivity to *p*-chlorophenylalanine (4-CP). Briefly, the IFDC2 cassette and homology
694 regions before and after the promoter of *SGO_2004* was amplified from an *S. gordonii*
695 strain containing IDFC2. PCR products were used as templates in a second PCR round
696 using only the external primers, which generated a linear dsDNA with the IFDC2 cas-
697 sette flanked by the upstream and downstream sequences. *Streptococcus gordonii*

bioRxiv preprint doi: https://doi.org/10.1101/2024.07.16.603716; this version posted July 16, 2024. The copyright holder for this preprint (which was not certified by peer review) is the author/funder, who has granted bioRxiv a license to display the preprint in perpetuity. It is made available under aCC-BY-NC-ND 4.0 International license.

698 DL1 WT was transformed with this construct and selected for insertion of the cassette
699 with erythromycin.
700 In a second time, the IDFC2 cassette was replaced by the P_{Tet} promoter of
701 pRPF185 plasmid fused with the pVeg RBS[50] by creating a construct with similar ho-
702 mologies regions than for the IFCD2 cassette or by using an homology region up-
703 stream of *padA* to create the Δ*padA,pTet-SGO_2004* mutant. After transformation of
704 *S. gordonii* IDFC2-DL1 with either construct, counter selection was done on BHI + *p*-
705 Cl-Phe plates and selected mutants verified by sanger sequencing and for sensibility
706 to erythromycin.
707

708 **Aggregation assay**

709 Overnight cultures were centrifuged for 5 min, 5000 g and resuspended in ag-
710 gregation buffer[23] (1 mM Tris- HCl buffer, pH 8.0, 0.1 mM $CaCl_2$, 0.1 mM $MgCl_2$, 150
711 mM NaCl) to a final OD_{600} of 1. 400 μL of each culture for co-aggregation or 800 μL
712 for auto-aggregation were added to a microspectrophotometer cuvette (Fisherbrand)
713 and left to sediment on the bench in the presence of oxygen, so no growth should
714 occur. The OD_{600} was measured every hour in a single point of the cuvette using a
715 SmartSpec spectrophotometer (Bio-Rad). OD_{600} were then normalized to the initial
716 OD_{600} by the formula.
717

718 **Purification of *SGO_2004* G5 domains**

719 The portion of *SGO_2004* coding for G5 domains (residues 138-698) was am-
720 plified from *S. gordonii* and the pET22b-HIS vector was linearized by PCR. The PCR
721 products were then purified and annealed by Gibson reaction. The plasmid was dia-
722 lyzed and transformed in electrocompetent *E. coli* DH5-alpha. After verification of the
723 construct by sequencing, the plasmid was purified and transformed in *E. coli*
724 BL21(DE3)-pDIA17. After growth to OD_{600} 0.4, cells were induced with 0.1 mM IPTG
725 and grown for 3h at 37°C before harvesting. Cell pellet was frozen O/N then resus-
726 pended in Buffer A (30 mM Tris-HCl pH 7.5, 300 mM NaCl, 30 mM Imidazole) and
727 lysed by sonication. Debris were pelleted by ultracentrifugation (50 000 g, 30 min) and
728 supernatant run through a HisTrap 5 mL column on an AKTA Explorer (GE) against a
729 gradient of imidazole (30-300 mM). The purified protein was assessed for purity by
730 SDS-Page followed by SafeStain SimplyBlue™ (ThermoFisher) staining and western

bioRxiv preprint doi: https://doi.org/10.1101/2024.07.16.603716; this version posted July 16, 2024. The copyright holder for this preprint (which was not certified by peer review) is the author/funder, who has granted bioRxiv a license to display the preprint in perpetuity. It is made available under aCC-BY-NC-ND 4.0 International license.

731 blot against the HIS-tag (Figure S10) and dialyzed twice against 30 mM Tris-HCl pH
732 7.5, 300 mM NaCl using a SnakeSkin™ 3500 Da (ThermoFisher).
733

734 **Immunofluorescence of surface bound $VisA_{G5}$**

735 *V. parvula* was grown overnight in SK and washed two times in PBS. $VisA_{G5}$
736 was preincubated 1 hour in the dark at 0.1 mg/mL with 1/10 of an anti-His Tag mono-
737 clonal antibody coupled with Alexa Fluor™ 488 (MA1-135-A488, Invitrogen). 50 µL of
738 bacteria at OD_{600} 1 was incubated for 2 hours with 5 µL of the fluorescent $VisA_{G5}$ and
739 subsequently mounted on a slide. Cells were imaged using a Zeiss Axioplan 2 micro-
740 scope equipped with an Axiocam 503 mono camera (Carl Zeiss, Germany). Epifluo-
741 rescence images were acquired using the ZEN lite software (Carl Zeiss, Germany) and
742 processed using Fiji (ImageJ).
743

744 **RNA extraction**

745 600 µL of anaerobic media BHIP (BHI + 100 mM sodium pyruvate) in a 1.5 mL
746 tube was inoculated with each of the bacteria at OD_{600} 0.05 and incubated for 6h an-
747 aerobically. Resulting culture was mixed with 1.2 mL of RNAprotect Bacteria reagent
748 (QIAGEN), vortexed and incubated at RT for 5 min, before centrifugation (10 000 rpm,
749 4°C) for 5 min. Supernatant was removed and pellet kept at -80°C before RNA extrac-
750 tion. For lysis, pellets were washed with 700 µL of PBS and resuspended in 200 µL of
751 lysis buffer (15 mg/mL Lysozyme, 100 µL / mL Proteinase K) before incubation for 3h
752 at 37°C with constant shaking (750 rpm). Each sample was then added to a matrix B
753 lysis tube with 800 µL of TRIzol and lysed using a FastPrep (2 times *S. mutans* pre-
754 registered protocol). 800 µL of 100% ethanol was added and samples were centrifuged
755 to pellet debris (8000 g, 2min). Lysate was transferred to a column from the kit Direct-
756 zol RNA Miniprep plus (Zymol) and the rest of the extraction was done following the
757 providers manual.
758

759 **RNA sequencing**

760 Libraries were prepared using Illumina Stranded Total RNA Prep from 440 ng of
761 RNA. RiboZero kit Microbiome kit (Illumina) was used to eliminate ribosomal RNA. The
762 subsequent steps were as follows: RNA fragmentation, cDNA synthesis (incorporating
763 uracils into the second strand), adapter ligation, indexing by PCR with 17 cycles
764 (amplifying only the first strand), purification of unbound adaptors and primers on AMP

bioRxiv preprint doi: https://doi.org/10.1101/2024.07.16.603716; this version posted July 16, 2024. The copyright holder for this preprint (which was not certified by peer review) is the author/funder, who has granted bioRxiv a license to display the preprint in perpetuity. It is made available under aCC-BY-NC-ND 4.0 International license.

765 beads (Beckman Coulter). The resulting stranded libraries comprised fragments from
766 200 to 1000 bp with peaks lying between 390 and 470 bp as visualized on a 5300
767 Fragment Analyzer (Agilent Technologies). No low-molecular peaks corresponding to
768 unbound adaptors and primer dimers were observed. Libraries were pooled and
769 sequenced on a NovaSeq X 10 B flow cell (Illumina) producing 1200 millions 150x150-
770 bp pair-end reads. As a result, each sample was represented by 18-55 million reads.
771 Ribofinder was used to verify the efficiency of ribodepletion: only around 5% of reads
772 mapped to ribosomal RNA. Taxonomy analysis using Kraken module confirmed the
773 presence of *S. gordonii* and *V. parvula* RNA according to the co-infection design. In
774 coinfection samples, reads from the two species were present in more or less equal
775 proportions. The RNA-seq analysis was performed with Sequana[51]. In particular, we
776 used the RNA-seq pipeline (v0.19.2, (https://github.com/sequana/sequana_rnaseq))
777 built on top of Snakemake v7.32.4[52]. Reads were trimmed from adapters and low-
778 quality bases using fastp software v0.22.0[53], then mapped to the reference genome
779 using Bowtie2 v2.4.6[54]. Genomes and annotations were downloaded from NCBI
780 website using *Veillonella parvula* SK38 (GenBank LR778174.1) and *S. gordonii* DL1
781 (GenBank CP000725.1) genome references. FeatureCounts 2.0.1[55] was used to
782 produce the count matrix, assigning reads to features using annotation
783 aforementioned. Statistical analysis on the normalized count matrix was performed to
784 identify differentially regulated genes. Differential expression testing was conducted
785 using DESeq2 library 1.34.0[56] scripts, and HTML reporting was made with the Sequana
786 RNA-seq pipeline.Parameters of the statistical analysis included the significance
787 (Benjamini-Hochberg adjusted p-values, false discovery rate FDR < 0.05) and the
788 effect size (fold-change) for each comparison.
789

790 **Confocal Laser Scanning Microscopy**

791 Biofilms were formed in a 96 well plate (PhenoPlate, PerkinElmer) by inoculating
792 150 µL of anaerobic media BHIP (BHI + 100 mM sodium pyruvate) with overnight cul-
793 ture of each species at OD_{600} 0.05 for each of them. After one hour of adhesion, media
794 was replaced to remove planktonic bacteria and incubated for 24 hours. Biofilm was
795 stained by addition of 50 µL of BHIP media containing both the BacGO (1 µM final
796 concentration) and the Syto61 dies (5 µM final concentration). Three images set at
797 defined positions within each well were acquired on an Opera Phenix Plus High

bioRxiv preprint doi: https://doi.org/10.1101/2024.07.16.603716; this version posted July 16, 2024. The copyright holder for this preprint (which was not certified by peer review) is the author/funder, who has granted bioRxiv a license to display the preprint in perpetuity. It is made available under aCC-BY-NC-ND 4.0 International license.

798 Content Screening System running with Harmony software v.5.1 (Revvity, formerly
799 known as PerkinElmer), using the following modalities: 20x water/NA 1.0, Z-stack, 40
800 planes, 2 μm step between planes, for the Syto61 dye: λ_{exc}: 640 nm / emission filter
801 650-760 nm), for the bacGO dye: λ_{exc}: 561 nm / emission filter 571-596 nm. Resulting
802 images were analyzed using BiofilmQ 1.0.1[57]. Images were first denoised by convolu-
803 tion (dxy = 5, dz = 3) and top hat filter (dxy= 25), then segmented in two classes using
804 an OTSU thresholding method with a sensitivity of 0.15 for the Syto61 channel and
805 0.25 for the BacGO channel. Images were then declumped in 10-pixel wide cubes and
806 Surface properties (range 30 pixel) and Global biofilm properties calculated (supple-
807 mentary data S3). Illustrative images were generated with Imaris 9.0.
808
809 **Data availability**
810
811 Supplementary data are available at
812 https://github.com/ldorison/Coaggregation_streptococcus_Veillonella-
813
814
815 **Acknowledgments**
816 We thank Mark Herzberg for sharing the bank of *S. gordonii* surface proteins mutants,
817 Justin Merritt for providing the *S. mutans* strains and the *S. gordonii* IDFC2 cassette,
818 Robert Smith for his help with using the AKTA and developing the *Veillonella* kanamy-
819 cin cassette and Bianca Audrain for developing the *Veillonella* erythromycin P_{Tet}-cas-
820 sette. We gratefully acknowledge the UTechS Photonic BioImaging (Imagopole),
821 C2RT, Institut Pasteur, supported by the French National Research Agency (France
822 BioImaging, ANR-10- INBS-04; Investments for the Future), and acknowledge support
823 from Institut Pasteur for the use of the Revvity Opera Phenix Plus microscope.
824
825 This work was supported by Institut Pasteur and grants by the French government's
826 Investissement d'Avenir Program, Laboratoire d'Excellence "Integrative Biology of
827 Emerging Infectious Diseases" (grant n°ANR-10-LABX-62-IBEID). L.D. was supported
828 by a MENESR (Ministère Français de l'Education Nationale, de l'Enseignement Supé-
829 rieur et de la Recherche) fellowship. C.M.G. was supported by a FRM Retour en
830 France fellowship. The RNA sequencing and analysis was performed by the Biomics
831 Platform, C2RT, Institut Pasteur, Paris, France, supported by France Génomique
832 (ANR-10-INBS-09-09).

bioRxiv preprint doi: https://doi.org/10.1101/2024.07.16.603716; this version posted July 16, 2024. The copyright holder for this preprint (which was not certified by peer review) is the author/funder, who has granted bioRxiv a license to display the preprint in perpetuity. It is made available under aCC-BY-NC-ND 4.0 International license.

833

834 **Contribution**

835 L.D., C.M.G. and C.B. designed the experiments. L.D., S.C., C.M.G., N.B., R.V., Y.V.
836 and R.O. performed the experiments. L.D. and C.B. wrote the paper, with contributions
837 from C.M.G., J.-M.G., N.B., R.O. and Y. V. and S.G. All authors read and approved the
838 manuscript.

839
840
841
842
843

844 **Bibliography**

845

846 1. Kolenbrander, P. E., Palmer, R. J., Periasamy, S. & Jakubovics, N. S. Oral multispecies
847 biofilm development and the key role of cell–cell distance. *Nature Reviews Microbiology* **8**,
848 471–480 (2010).
849 2. Kolenbrander, P. E. *et al.* Bacterial interactions and successions during plaque devel-
850 opment. *Periodontol 2000* **42**, 47–79 (2006).
851 3. Kolenbrander, P. E., Ganeshkumar, N., Cassels, F. J. & Hughes, C. V. Coaggregation:
852 specific adherence among human oral plaque bacteria. *The FASEB Journal* **7**, 406–413 (1993).
853 4. Afonso, A. C. *et al.* Bacterial coaggregation in aquatic systems. *Water Research* **196**,
854 117037 (2021).
855 5. Hajishengallis, G., Lamont, R. J. & Koo, H. Oral polymicrobial communities: Assembly,
856 function, and impact on diseases. *Cell Host & Microbe* (2023)
857 doi:10.1016/j.chom.2023.02.009.
858 6. Mohanty, R. *et al.* Red complex: Polymicrobial conglomerate in oral flora: A review. *J*
859 *Family Med Prim Care* **8**, 3480–3486 (2019).
860 7. Hughes, C. V., Kolenbrander, P. E., Andersen, R. N. & Moore, L. V. Coaggregation
861 properties of human oral Veillonella spp.: relationship to colonization site and oral ecology.
862 *Applied and Environmental Microbiology* (1988) doi:10.1128/aem.54.8.1957-1963.1988.
863 8. Zhou, P., Manoil, D., Belibasakis, G. N. & Kotsakis, G. A. Veillonellae: Beyond Bridging
864 Species in Oral Biofilm Ecology. *Frontiers in Oral Health* **2**, (2021).
865 9. Kaplan, C. W., Lux, R., Haake, S. K. & Shi, W. The Fusobacterium nucleatum outer
866 membrane protein RadD is an arginine-inhibitable adhesin required for inter-species adher-
867 ence and the structured architecture of multispecies biofilm. *Mol. Microbiol.* **71**, 35–47
868 (2009).
869 10. Takemoto, T. *et al.* Characteristics of multimodal co-aggregation between Fusobacte-
870 rium nucleatum and streptococci. *Journal of Periodontal Research* **30**, 252–257 (1995).
871 11. Guo, L., Shokeen, B., He, X., Shi, W. & Lux, R. Streptococcus mutans SpaP Binds to
872 RadD of Fusobacterium nucleatum ssp polymorphum. *Mol Oral Microbiol* **32**, 355–364
873 (2017).
874 12. Periasamy, S. & Kolenbrander, P. E. Central Role of the Early Colonizer Veillonella sp.
875 in Establishing Multispecies Biofilm Communities with Initial, Middle, and Late Colonizers of
876 Enamel. *Journal of Bacteriology* **192**, 2965–2972 (2010).

bioRxiv preprint doi: https://doi.org/10.1101/2024.07.16.603716; this version posted July 16, 2024. The copyright holder for this preprint (which was not certified by peer review) is the author/funder, who has granted bioRxiv a license to display the preprint in perpetuity. It is made available under aCC-BY-NC-ND 4.0 International license.

877 13. Chung, W. O., Demuth, D. R. & Lamont, R. J. Identification of a Porphyromonas gingi-
878 valis receptor for the Streptococcus gordonii SspB protein. *Infect Immun* **68**, 6758–6762
879 (2000).
880 14. Maeda, K. *et al.* Glyceraldehyde-3-Phosphate Dehydrogenase of Streptococcus oralis
881 Functions as a Coadhesin for Porphyromonas gingivalis Major Fimbriae. *Infection and Im-*
882 *munity* **72**, 1341–1348 (2004).
883 15. Coppenhagen-Glazer, S. *et al.* Fap2 of Fusobacterium nucleatum Is a Galactose-Inhib-
884 itable Adhesin Involved in Coaggregation, Cell Adhesion, and Preterm Birth. *Infection and Im-*
885 *munity* **83**, 1104–1113 (2015).
886 16. Giacomini, J. J., Torres-Morales, J., Dewhirst, F. E., Borisy, G. G. & Mark Welch, J. L.
887 Site Specialization of Human Oral Veillonella Species. *Microbiol Spectr* e0404222 (2023)
888 doi:10.1128/spectrum.04042-22.
889 17. Delwiche, E. A., Pestka, J. J. & Tortorello, M. L. THE VEILLONELLAE: GRAM-NEGATIVE
890 COCCI WITH A UNIQUE PHYSIOLOGY. *Annual Review of Microbiology* **39**, 175–193 (1985).
891 18. Egland, P. G., Palmer, R. J. & Kolenbrander, P. E. Interspecies communication in Strep-
892 tococcus gordonii–Veillonella atypica biofilms: Signaling in flow conditions requires juxtapo-
893 sition. *PNAS* **101**, 16917–16922 (2004).
894 19. Johnson, B. P. *et al.* Interspecies Signaling between Veillonella atypica and Strepto-
895 coccus gordonii Requires the Transcription Factor CcpA. *J Bacteriol* **191**, 5563–5565 (2009).
896 20. Zhou, P., Li, X., Huang, I.-H. & Qi, F. Veillonella Catalase Protects the Growth of Fuso-
897 bacterium nucleatum in Microaerophilic and Streptococcus gordonii-Resident Environments.
898 *Applied and Environmental Microbiology* **83**, e01079-17 (2017).
899 21. Hughes, C. V., Andersen, R. N. & Kolenbrander, P. E. Characterization of Veillonella
900 atypica PK1910 adhesin-mediated coaggregation with oral Streptococcus spp. *Infect Immun*
901 **60**, 1178–1186 (1992).
902 22. Hughes, C. V., Roseberry, C. A. & Kolenbrander, P. E. Isolation and characterization of
903 coaggregation-defective mutants of *Veillonella atypica*. *Archives of Oral Biology* **35**, S123–
904 S125 (1990).
905 23. Zhou, P., Liu, J., Merritt, J. & Qi, F. A YadA-like autotransporter, Hag 1, in Veillonella
906 atypica is a Multivalent Hemagglutinin Involved in Adherence to Oral Streptococci, Porphy-
907 romonas gingivalis, and Human Oral Buccal Cells. *Mol Oral Microbiol* **30**, 269–279 (2015).
908 24. Zhou, P., Liu, J., Li, X., Takahashi, Y. & Qi, F. The Sialic Acid Binding Protein, Hsa, in
909 Streptococcus gordonii DL1 also Mediates Intergeneric Coaggregation with Veillonella Spe-
910 cies. *PLOS ONE* **10**, e0143898 (2015).
911 25. Béchon, N. *et al.* Autotransporters Drive Biofilm Formation and Autoaggregation in
912 the Diderm Firmicute Veillonella parvula. *Journal of Bacteriology* **202**, (2020).
913 26. Nairn, B. L. *et al.* Uncovering Roles of Streptococcus gordonii SrtA-Processed Proteins
914 in the Biofilm Lifestyle. *Journal of Bacteriology* **203**, (2020).
915 27. Petersen, H. J. *et al.* Human Platelets Recognize a Novel Surface Protein, PadA, on
916 Streptococcus gordonii through a Unique Interaction Involving Fibrinogen Receptor GPIIbIIIa.
917 *Infect Immun* **78**, 413–422 (2010).
918 28. Biswas, I., Jha, J. K. & Fromm, N. Shuttle expression plasmids for genetic studies in
919 Streptococcus mutans. *Microbiology (Reading)* **154**, 2275–2282 (2008).
920 29. Mutha, N. V. R. *et al.* Transcriptional profiling of coaggregation interactions between
921 Streptococcus gordonii and Veillonella parvula by Dual RNA-Seq. *Scientific Reports* **9**, 7664
922 (2019).
923 30. Jakubovics, N. S., Gill, S. R., Iobst, S. E., Vickerman, M. M. & Kolenbrander, P. E.

bioRxiv preprint doi: https://doi.org/10.1101/2024.07.16.603716; this version posted July 16, 2024. The copyright holder for this preprint (which was not certified by peer review) is the author/funder, who has granted bioRxiv a license to display the preprint in perpetuity. It is made available under aCC-BY-NC-ND 4.0 International license.

924 Regulation of Gene Expression in a Mixed-Genus Community: Stabilized Arginine Biosynthe-
925 sis in Streptococcus gordonii by Coaggregation with Actinomyces naeslundii. *Journal of Bac-*
926 *teriology* **190**, 3646–3657 (2008).
927 31. Development of a Universal Fluorescent Probe for Gram-Positive Bacteria - Kwon -
928 2019 - Angewandte Chemie International Edition - Wiley Online Library. https://onlineli-
929 brary.wiley.com/doi/full/10.1002/anie.201902537.
930 32. Takahashi, Y., Konishi, K., Cisar, J. O. & Yoshikawa, M. Identification and Characteriza-
931 tion of hsa, the Gene Encoding the Sialic Acid-Binding Adhesin of Streptococcus gordonii
932 DL1. *Infection and Immunity* **70**, 1209–1218 (2002).
933 33. Haworth, J. A. *et al.* Concerted functions of Streptococcus gordonii surface proteins
934 PadA and Hsa mediate activation of human platelets and interactions with extracellular ma-
935 trix. *Cellular Microbiology* **19**, e12667 (2017).
936 34. Béchon, N. *et al.* Capsular Polysaccharide Cross-Regulation Modulates Bacteroides
937 thetaiotaomicron Biofilm Formation. *mBio* **11**, e00729-20 (2020).
938 35. Bateman, A., Holden, M. T. G. & Yeats, C. The G5 domain: a potential N-acetylglu-
939 cosamine recognition domain involved in biofilm formation. *Bioinformatics* **21**, 1301–1303
940 (2005).
941 36. Corrigan, R. M., Rigby, D., Handley, P. & Foster, T. J. The role of Staphylococcus au-
942 reus surface protein SasG in adherence and biofilm formation. *Microbiology (Reading)* **153**,
943 2435–2446 (2007).
944 37. Mutha, N. V. R. *et al.* Transcriptional responses of Streptococcus gordonii and Fuso-
945 bacterium nucleatum to coaggregation. *Mol Oral Microbiol* **33**, 450–464 (2018).
946 38. Kiliç, A. O. *et al.* Involvement of Streptococcus gordonii Beta-Glucoside Metabolism
947 Systems in Adhesion, Biofilm Formation, and In Vivo Gene Expression. *Journal of Bacteriol-*
948 *ogy* **186**, 4246–4253 (2004).
949 39. Jakubovics, N. S. *et al.* Critical roles of arginine in growth and biofilm development by
950 Streptococcus gordonii. *Molecular Microbiology* **97**, 281–300 (2015).
951 40. Liu, J., Wu, C., Huang, I.-H., Merritt, J. & Qi, F. Differential response of Streptococcus
952 mutans towards friend and foe in mixed-species cultures. *Microbiology (Reading)* **157**, 2433–
953 2444 (2011).
954 41. Luppens, S. B. I. *et al.* Effect of Veillonella parvula on the antimicrobial resistance and
955 gene expression of Streptococcus mutans grown in a dual-species biofilm. *Oral Microbiology*
956 *and Immunology* **23**, 183–189 (2008).
957 42. Chekli, Y. *et al.* Escherichia coli Aggregates Mediated by Native or Synthetic Adhesins
958 Exhibit Both Core and Adhesin-Specific Transcriptional Responses. *Microbiol Spectr* **11**,
959 e0069023 (2023).
960 43. Sønderholm, M. *et al.* Pseudomonas aeruginosa Aggregate Formation in an Alginate
961 Bead Model System Exhibits In Vivo-Like Characteristics. *Applied and Environmental Microbi-*
962 *ology* **83**, e00113-17 (2017).
963 44. Nadell, C. D., Drescher, K., Wingreen, N. S. & Bassler, B. L. Extracellular matrix struc-
964 ture governs invasion resistance in bacterial biofilms. *ISME J* **9**, 1700–1709 (2015).
965 45. Burmølle, M. *et al.* Enhanced Biofilm Formation and Increased Resistance to Antimi-
966 crobial Agents and Bacterial Invasion Are Caused by Synergistic Interactions in Multispecies
967 Biofilms. *Appl Environ Microbiol* **72**, 3916–3923 (2006).
968 46. Lee, K. W. K. *et al.* Biofilm development and enhanced stress resistance of a model,
969 mixed-species community biofilm. *ISME J* **8**, 894–907 (2014).
970 47. Knapp, S. *et al.* Natural Competence Is Common among Clinical Isolates of Veillonella

bioRxiv preprint doi: https://doi.org/10.1101/2024.07.16.603716; this version posted July 16, 2024. The copyright holder for this preprint (which was not certified by peer review) is the author/funder, who has granted bioRxiv a license to display the preprint in perpetuity. It is made available under aCC-BY-NC-ND 4.0 International license.

971 parvula and Is Useful for Genetic Manipulation of This Key Member of the Oral Microbiome.
972 *Front. Cell. Infect. Microbiol.* **7**, (2017).
973 48. Danne, C., Guérillot, R., Glaser, P., Trieu-Cuot, P. & Dramsi, S. Construction of isogenic
974 mutants in Streptococcus gallolyticus based on the development of new mobilizable vectors.
975 *Research in Microbiology* **164**, 973–978 (2013).
976 49. Zhang, S., Zou, Z., Kreth, J. & Merritt, J. Recombineering in Streptococcus mutans Us-
977 ing Direct Repeat-Mediated Cloning-Independent Markerless Mutagenesis (DR-CIMM). *Front*
978 *Cell Infect Microbiol* **7**, 202 (2017).
979 50. Shields, R. C., Kaspar, J. R., Lee, K., Underhill, S. a. M. & Burne, R. A. Fluorescence
980 Tools Adapted for Real-Time Monitoring of the Behaviors of Streptococcus Species. *Appl. En-*
981 *viron. Microbiol.* **85**, (2019).
982 51. Cokelaer, T., Desvillechabrol, D., Legendre, R. & Cardon, M. 'Sequana': a Set of Snake-
983 make NGS pipelines. *Journal of Open Source Software* **2**, 352 (2017).
984 52. Köster, J. & Rahmann, S. Snakemake—a scalable bioinformatics workflow engine. *Bio-*
985 *informatics* **28**, 2520–2522 (2012).
986 53. Chen, S., Zhou, Y., Chen, Y. & Gu, J. fastp: an ultra-fast all-in-one FASTQ preprocessor.
987 *Bioinformatics* **34**, i884–i890 (2018).
988 54. Langmead, B. & Salzberg, S. L. Fast gapped-read alignment with Bowtie 2. *Nat Meth-*
989 *ods* **9**, 357–359 (2012).
990 55. Liao, Y., Smyth, G. K. & Shi, W. featureCounts: an efficient general purpose program
991 for assigning sequence reads to genomic features. *Bioinformatics* **30**, 923–930 (2014).
992 56. Love, M. I., Huber, W. & Anders, S. Moderated estimation of fold change and disper-
993 sion for RNA-seq data with DESeq2. *Genome Biology* **15**, 550 (2014).
994 57. Hartmann, R. *et al.* Quantitative image analysis of microbial communities with Bio-
995 filmQ. *Nat Microbiol* **6**, 151–156 (2021).
996